AMERICAN UNIVERSITY OF BEIRUT

DYNAMIC ASSESSMENT AND FEM MODELING OF THE MODAL FREQUENCIES AND SHAPES OF BOVINE TIBIA BONE

by
REEM ALI YASSINE

A thesis
submitted in partial fulfillment of the requirements
for the degree of Master of Engineering
to the Department of Mechanical Engineering
of the Maroun Semaan Faculty of Engineering and Architecture
at the American University of Beirut

Beirut, Lebanon
August 2018

AMERICAN UNIVERSITY OF BEIRUT

DYNAMIC ASSESSMENT AND FEM MODELING OF THE MODAL FREQUENCIES AND SHAPES OF BOVINE TIBIA BONE

by

REEM ALI YASSINE

Approved by:

Ramsey Hamade, Professor
Department of the Mechanical Engineering
_____ Advisor

Samir Mustapha, Assistant Professor _____
Department of the Mechanical Engineering Member of Committee

Mohammad Harb, Assistant Professor _____
Department of the Mechanical Engineering Member of Committee

Date of thesis defense: August 7, 2018

AMERICAN UNIVERSITY OF BEIRUT

THESIS, DISSERTATION, PROJECT RELEASE FORM

Student Name:

Yassine	Reem	Ali
Last	First	Middle

● Master's Thesis ○ Master's Project ○ Doctoral Dissertation

■ I authorize the American University of Beirut to: (a) reproduce hard or electronic copies of my thesis, dissertation, or project; (b) include such copies in the archives and digital repositories of the University; and (c) make freely available such copies to third parties for research or educational purposes.

☐ I authorize the American University of Beirut, to: (a) reproduce hard or electronic copies of it; (b) include such copies in the archives and digital repositories of the University; and (c) make freely available such copies to third parties for research or educational purposes after:

One ---- year from the date of submission of my thesis, dissertation, or project.
Two ---- years from the date of submission of my thesis, dissertation, or project.
Three ---- years from the date of submission of my thesis, dissertation, or project.

August 27th , 2018

Signature Date

ACKNOWLEDGMENTS

I express my deep thanks and gratitude to God for giving us the chance to seek knowledge. I am grateful to AUB for granting me the opportunity to apply and demonstrate the given cognition through the Master's Program in Mechanical Engineering. Foremost, I would like to thank my advisor Prof. Ramsey Hamade for the valuable guidance and advice. He inspired me greatly in our work with his constant support and creative ideas.

This work was made possible by Award #103087 from the Lebanese National Council for Scientific Research. The authors also acknowledge the financial support of the university research board (URB) at the American University of Beirut.

AN ABSTRACT OF THE THESIS OF

Reem Ali Yassine for Master of Engineering
Major: Mechanical Engineering

Title: Dynamic Assessment and FEM Modeling of the Modal Frequencies and Shapes of Bovine Tibia Bone

Frequency response function (FRF) and Complex Mode Indicator Function (CMIF) techniques were used to experimentally measure the modal frequencies for several long (bovine) tibia bones. CMIF has an advantage of detecting closely spaced modes by excluding misinterpreted peaks. It was found that the difference between the two methods did not exceed 2.98 %. CMIF data was more consistent when varying impact location. Effect of bone's geometrical attributes on modal frequencies was statistically scrutinized and highly correlated parameters were identified. Bone length exhibited high correspondence to frequencies ($p < 0.05$) for practically all modes. Also, four simple equations were developed, relating modes 1 and 2 in the cranial-caudal (C-C) and medial-lateral (M-L) planes to the characteristic length of the bone.
Starting from anatomically accurate computed tomography (CT) scans, the finite elements method (FEM) using ANSYS was employed to numerically estimate the modal frequencies of the same experimentally-characterized long (bovine) tibia bones. Accurate results require the proper selection of stiffness versus density (E-ρ) formulae for both cortical and cancellous bone constituents. This work uncovered and tested 22 literature-reported formulae to assign elemental stiffness relative to stiffness–density relations. Bones are segmented into their cortical and cancellous constituents according to found suitable values of three variables: 1) critical cut-off Hounsfield (HU), 2) cut-off density, and 3) utilized number of materials. These variables were found by replicating the bone actual mass. Numerically estimated modal frequencies are compared to those measured from our dynamic experiments. Out of the 22 literature-reported formulae considered, the most accurate formulae yielded numerical estimates with errors (percentage difference between experimental data and FEM solution) of 0.95% and 10.65% for 1st and 2nd cranial-caudal (C-C) frequencies, respectively.

CONTENTS

ILLUSTRATIONS

TABLES

CHAPTER I

INTRODUCTION

Biomedical engineering has become a leading field in the development of new technologies that play a major role in body health assessment such as the MRI (Magnetic Resonance Imaging) and CT scan (Computerized Tomography). Over the past decade, Biomedical Engineering has been continuously providing the medical field with solutions to rigorous health issues that have become very prominent in the population, some of these health issues include CVD (Cardiovascular Disease) [1], lung failure, and bone-related diseases such as Osteopenia and Osteoporosis. The non-invasive assessment of bone biomechanical competence remains a challenge, despite the ever-growing number of physical and imaging tools available. The assessment of the effect of bone metabolic diseases on the mechanical properties of long bones, such as tibia, is associated with several challenges related to the limitations of the current methods in use [2]. In relation to Osteoporosis, the variation in the flexural and torsional stiffness of long bones, highly depends on the geometrical nature of the bones and the encasing tissues around it. Modal parameter identification is a practical tool that has long been employed in characterizing the dynamic behavior of complex structures. Determining physical properties of long bones by determining resonant frequencies is not new [3, 4], and was later proposed for long bones [5]. Many research work has been done in the field of bone characterization to serve the purpose of relating dynamic properties of a bone to the modes of vibration.

A greater interest was developed for predicting the mechanical properties of bones using 3D finite element method (FEM) from quantitative computed tomography

(CT) [6, 7] or micro-CT (μCT) [8, 9] or X-rays [10] and the computations of natural frequencies. CT scans (Computerized Topography) is a biomedical technology utilized in diagnosing and locating severe bone diseases and fractures. The key for accurate numerical (FEM) results of biomedical studies, lies in developing an accurate 3D anatomical model and assigning proper material properties. Different human/animal anatomical structures were examined in that context, as human tibia [11, 12], human femur [13, 14] and human mandible or teeth [15, 16].

For cancellous and cortical constituents of long bone, there exists in the literature a large number of stiffness vs. apparent density (E-ρ) formulations of various forms. We wish to establish a methodology for disambiguating the salient features of such equations so that their use in clinical applications would have merit. To this end, Yassine et al. [17] compared three cases of different E-ρ relations for the purpose of comparing the heterogeneous material considerations to homogenous for obtaining accurate and efficient estimates of modal frequencies in long bones. It was found that heterogeneous material considerations of bone yielded more accurate modal frequency estimates when compared to experimental vibrational measurements. The work is extended here by using heterogeneous material for a large number of combinations for E-ρ equations. For this purpose, this work surveys and critically assesses such formulae in the context of being able to predict the bone' frequency values. Included in the surveyed formulae are only those relevant to bone characterization via computerized tomography (CT) scans (e.g., Hounsfield units (HU) as variable), experimentally and analytically. Said values are later compared against experimentally measured frequency values in separate dynamic assessment work performed by Hamade and coauthors.

This work employs the Complex Mode Indicator function (CMIF) on Experimental Modal Analysis (EMA) data, as it is capable of capturing real and imaginary modes [18] and detecting closely spaced modes unlike other MIFs [19]. Furthermore, EMA is examined utilizing a Fast Fourier Transform (FFT) analyzer in order to determine the frequency response function (FRF) used to study the dynamic properties of bovine tibia. The authors first examine the applicability of CMIF in determining the vibrational characteristics of a large number (13) of long bones (bovine tibia) assessed *in vitro* by impact testing. Impact testing has an advantage in going across frequencies more efficiently [20] than other techniques. The bones were instrumented with single axis accelerometers distributed uniformly over the length of the bone, and then were impacted at different locations in the Cranial-Caudal and Medial-Lateral planes, to identify the modal frequencies. FRF data and CMIF were used to identify the modal frequencies. Comparisons were made of the extracted modal frequencies based on the two approaches.

Second, we survey and list much of the literature-reported stiffness vs. density formulae for both cancellous and cortical constituents of long bones with critical assessment of their biological and material collection methods and conditions. The study is employed to compute the 1st and 2nd modal frequency values in both the cranial-caudal and medial-lateral planes of bovine tibia bone. After the bone is CT-scanned, Mimics software [21] is used to transform the data to a 3D model. Apparent density values are linearly related to the CT number (Hounsfield Unit, HU). In 22 different what-if-cases based on the surveyed equations, meshed elements' stiffness is computed as function of density. All cases were run as linearly elastic, isotropic and heterogeneous materials. Elements are assigned as being either cortical or cancellous

based on cutoff–HU value converged upon by digitally replicating the bone mass. The study proceeds to identify those literature-reported formulae that come closest to predicting the modal frequencies and shapes of bovine tibia bone as compared to experimental measurements (made by Hamade and coworkers [22, 23] where the first and second natural frequencies were identified by the frequency response function (FRF).

Third, the study develop simple equations that estimate modal frequencies as function of bone lengths as the lone required variable. For this purpose, the effects of several geometrical parameters on the modal frequencies were scrutinized, and the highly correlated parameters were identified and retained. On this basis, geometrical models were developed for modal frequency estimation. For bone mode shapes, six of the long tibias were dynamically characterized using the frequency response function (FRF) data extracted using ProSig© software.

CHAPTER II

LITERATURE

Characterizing the mechanical properties of long bones, such as tibia, is associated with several challenges related to the limitations of the methods employed including those by vibration and ultrasonic techniques [2]. Dynamic response in the assessment of mechanical properties of long bones was early proposed by Doherty [3]. Numerous research has been conducted in the field of bone characterization to serve the purpose of relating dynamic properties of a bone to vibration modes [5, 24]. Various analysis techniques were developed to extract dynamic data (modal frequencies, damping ratio, and mode shapes) and simulate physical models. Some of such techniques are Experimental Modal Analysis (EMA), Operational Modal Analysis (OMA), and Finite Element Analysis (FEA).

Sonstegard and Matthews [5] employed vibrational studies evaluated the correspondence of fracture healing to (in situ) modal frequencies of long bones. Cornelissen et al. [25] conducted vibration experiments to determine the modal frequencies and their relative mode shapes. Van der Perre et al. [24] experimentally determined the modal parameters of human tibia in different cases. The cases include excised tibias (dry and fresh), *in-vivo* tibia and a sample extracted from an amputated leg. Lowet and coworkers [2, 26] utilized vibration- and ultrasound-based methods for their study on bone characterization. In their experiments, they used dog femora for in vitro experiments and human tibia for in vivo experiments. They concluded that both methods of analysis permit the discrimination amid geometrical changes and material property changes, in which the evaluation of the ultrasound attenuation provides

significant information on the structure of trabecular bone. Whilst the vibration analysis creates the relationship between long bone mechanical properties and the factors affecting these properties. Further, the work of Christensen et al. [27] and Nakatsuchi et al. [28] focused on clarifying the use of the impulse response method in the assessment of fracture healing. It was found [28] that the consolidation process of a material in a fracture gap can be assessed by the overall change of resonant frequency of the bone, thus, a quantitative assessment of fracture healing can be achieved. Alizad et al. [29] determined the vibrational characteristics of small long bones (for a rat) by observing the variation in resonant frequencies remotely and noninvasively. The study was done by exerting a vibrating force using a certain amplitude-modulated ultrasound. The change indicates the health condition of the bone, whether it is healing or fractured. Similar work by Nokes et al. [30] was carried to develop a quantitative method that can assess fracture healing. Their experimental setup was based on intact human tibia, a 28-g steel ball that was dropped onto the tibial tubercle through a tube as means of excitation, and an accelerometer that measured the response at two different positions on the bone (one distal to the tibial tubercle and the other proximal to the medial malleolus). Hight et al. [31] focused on modeling human tibia. Their work compared analytical and experimental solutions to that acquired from a beam type finite element numerical model that predicts natural frequency response of a human tibia with varying properties. It was found that the values of natural frequencies are highly influenced by boundary conditions. Work by Collier et al. [32] focused on validating a simple beam model for predicting torsional stiffness from resonant frequencies with the aid of vibrational experiments and impact torsion tests. Their setup comprised of monkey radii, sheep femurs, dog tibiae, and dog femurs, an impact hammer for excitation, a

microphone for signal reception, and a spectrum analyzer for data analysis. A relationship was established between torsional stiffness and resonant frequencies of single bending modes, mass and bone length, based on a simple uniform slender beam model. Nevertheless, it was noted that using this model to predict resonant frequencies in bones is valid only for the first vibration modes. A study by Thomsen [12] used human tibia to extract seven tibial frequencies between 0-3000 Hz. Those frequencies correspond to six flexural mode shapes and one torsional mode. This tibial bone was modeled with Timoshenko beam type capable of predicting more natural frequencies. Wang and Williams [33] classified the vibrational modes into pure and non-pure radial modes considering the effect of varying both radial and axial dimensions on modal frequencies.

Regarding modal frequencies extraction, the direct use of modal parameters based on Fast Fourier Transform (FFT) may be challenging given that the modal data are not broadband data (cover only a limited number of FRF data around the resonant frequencies). Modal data may lack accuracy due to modal extraction processing. On the other hand, FRF data are less error prone because they are directly extracted from the responses. Furthermore, they include abundant information in a wide range of frequencies [34, 35]. Liu et al. [36] proposed a method to predict and control vibrations on a specific location of a building structure due to impact loading. The loading was examined for cases done by a hammer or a blast, and are simplified as an impulse train. The authors described it as a simpler non-linear method for nonlinear systems, modeled by Volterra functional series. In situ experiments were done and compared to the calculated results, and were in a good agreement. Malekian et al. [20] aimed to study the mechanical behavior of bovine spine by EMA. Natural frequencies of the

intervertebral disk were extracted using impact testing technique. The intervertebral substructures (joints) were mathematically coupled using the receptance coupling method at the extracted frequency values. Alternatively, Mode Indicator Functions (MIFs) are real-valued frequency-dependent scalars that exhibit local minima or maxima at system's modal frequencies [37]. There exist many types of MIFs, and their relevance to the experimental work depends on the nature and complexity of the system under consideration. Some MIFs include: Multivariate Mode Indicator Function (MMIF), Complex Mode Indicator Function (CMIF), U-Mode Indicator Function (UMIF), Component wise Mode Indicator Function (CoMIF), and Q-Vector Component wise Mode Indicator Function (QCoMIF) [37]. Phillips et al. [38] discussed different modal parameters estimation algorithms some of which are Complex Exponential Algorithm, Eigensystem Realization Algorithm, Multi-Reference Frequency Domain, and the Complex Mode Indicator Function. It was stated that the CMIF (zeroth-order algorithm) provides direct estimates of the eigenvectors and is commonly used to process obtained data at a single or variable temporal conditions. The peak in the CMIF plot signifies the location on the frequency axis that is closest to the pole. The closer the modal frequency is to the discrete frequency, the higher the singular value will be [38]. Hence, it can detect closely spaced modes [39] and of capturing real and imaginary modes [18].

Early numerical and analytical studies have been conducted to compute the natural frequencies of human tibia. Thomsen [12] approximated long bones as beam finite model and estimated frequency values of 431 Hz and 520 Hz for the first modes and 1220 Hz and 1489 Hz for the second modes associated with anterior-posterior and medial-lateral planes, respectively. Hobatho et al. [11] obtained a 3% difference

between the two outcomes upon considering inhomogeneous material. The first natural frequencies were around 421.25 Hz and 505.5 Hz, and the second natural frequencies were approximately 1096.5 Hz and 1272 Hz. It was found that the difference is due to the assigned mechanical properties and mass distribution. Lowet [26] studied the first modal frequency for various animal species (sheep, dogs and monkeys) by which specimens were modeled as a uniform slender beam model.

To relate bone stiffness to behavior, a large number of stiffness vs. density equations can be found in the biomechanics literature developed using a variety of methods. Employing three-point bending tests, Snyder and Schneider [40] proposed formulation for the mid-diaphysis region of human tibia bones being of 29-73 years old, by examining 45 flat rectangular (slices) specimens. Based on the theory of thin plates, a study of human long bones by Lotz et al. [41] included both metaphyseal and diaphyseal regions with 123 and 36 tested specimens, respectively. While employing 38 specimens, a stiffness-density linear relation was formulated by Keaveny et al. [42] for cancellous tibia bone in the proximal region. Gupta and Dan [43] established relations for human scapula bone using a relatively large number (25) of data points with only 2 points used for cortical bone extracted from the subchondral region. Wirtz et al. [44] formulated E-ρ relations by computing the mean regression line of earlier works by Abendschein and Hyatt [45] and Lotz et al. [41]. Austman et al. [46] compared customized equations against experimental (using 12 uniaxial strain gauges) outcomes describing 8 long ulna bones harvested from distal regions. Austman et al. [47] examined six various literature-reported relations based on human ulnae. Contrasting to previous experimental work on strain and perhaps due to high estimates of cortical stiffness, only 2 equations were selected with one [48] under-estimating and the other

[49] over-estimating strain target values. Other [47, 50] used extrapolations of the same equation to cover density ranges of cortical and cancellous constituents. Reported formulations of cortical and cancellous bovine bone include those by Huang et al. [51] and Keaveny et al. [42]. Using 10 bovine femur diaphyseal cortical bone, Huang et al. [51] related the stiffness modulus to CT number (Gray values (GV)) by matching experimental and numerical results of compressive tests.

CHAPTER III

EXPERIMENTAL WORK

A. Setup

Thirteen fresh bovine tibia bones were collected from different calves approximately 2 years of age collected fresh from butcher. The cleaning process employed Bio-powder that contained enzymes to help remove extra surface tissues. The bones were tested in a free-free setup scenario (Figure 1) where they rested on rubber supports that were attached at one end to the surface of a damping table (Newport Lab Legs™ RL- 2000 series) by means of bolts, and at the other end to the bone extremities. The case of a free-free system best describes the actual anatomical boundary conditions of the bone, despite eliminating preloading [52]. By hanging the bones as such during the experiments, external loads other than the tension acting on the supports were eliminated, and the free-free boundary condition was ensured [53]. The experimental setup comprises of an impact hammer (Dynapulse™ Impulse Hammer) with a hard plastic tip and six accelerometers mounted using wax (Figure 1). Accelerometers on locations 1, 3, 4 and 6 (PCB Piezoelectronics 352C34 SN) that are equally spaced, were employed in the modal frequency study. Three distinct impact locations were chosen for excitation such that the first is located between accelerometers 1 and 3, the second is between accelerometers 3 and 4, and the third is between accelerometers 4 and 6 as indicated in Figure 1.

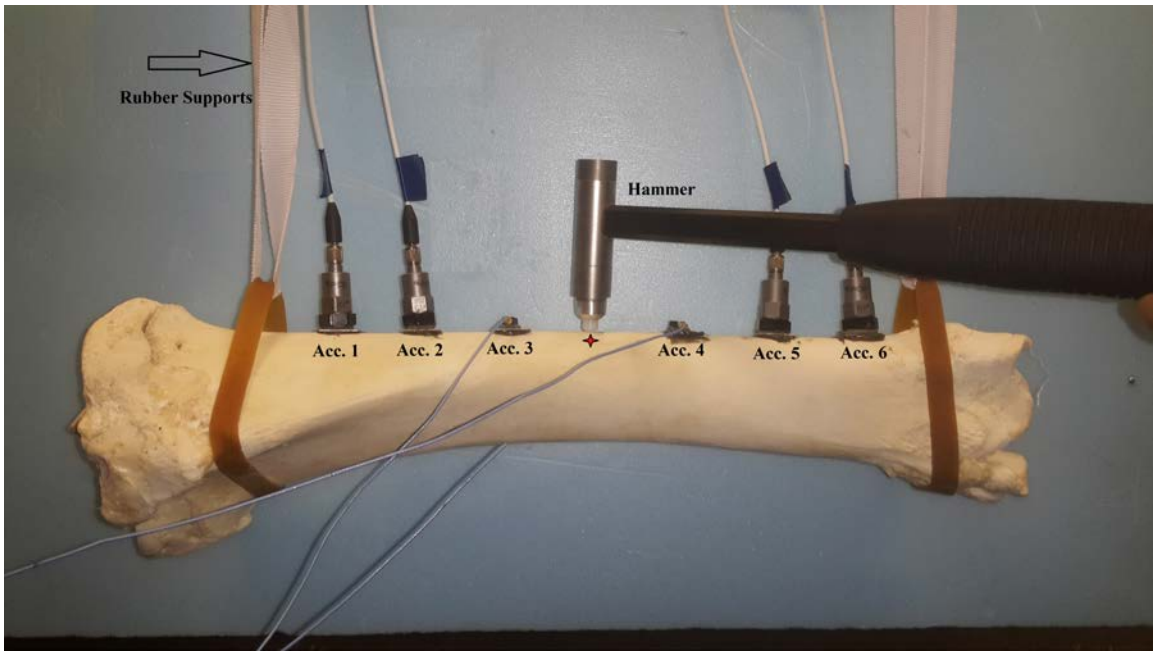

Figure 1. Experimental set-up for mode shape (medial-lateral plane shown).

For the mode shapes study, a variant of this procedure using additional accelerometers was used. Accelerometers 3 and 4 (PCB Piezoelectronics 352C22 SN) have low sensitivity (~10 mV/g) and are very lightweight (0.5 grams). Accelerometers 1, 2, 5 and 6 (PCB Piezoelectronics 352C34 SN) have higher sensitivity (~100 mV/g) and are 5.8 grams each. Vibrations were excited by an impact hammer (Dynapulse™ Impulse Hammer) at a single point located at mid-span. This study is employed on Bones 6, 8, 10, 11, 12, and 13.

Bone's geometric parameters were measured in the Cranial-Caudal and Medial-Lateral planes for two sectioned regions (Figure 2a and 2b). Table 1 lists the measured geometrical attributes. The bone was assumed to have an elliptical cross-sectional area [54] to ease the calculation of geometrical parameters such as mid-section area and perimeter. The Cranial-Caudal distance (CC) and Medial-Lateral distance

(ML) are the primary distances of section BB, and d_{CC} and d_{ML} are the primary diameters of section AA.

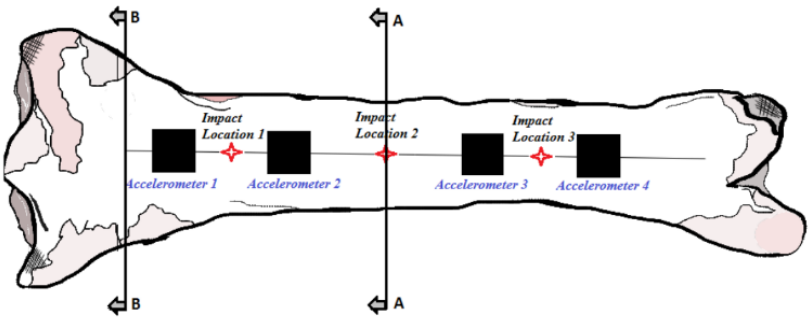

Figure 2a. Two respective cross sections B-B and A-A used for dimensional measurements.

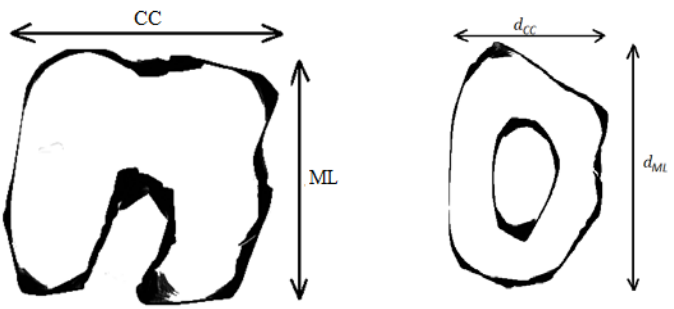

Figure 2b. Sections BB and AA respectively from left to right.

Table 1. Dimensional measurements of tibia bones.

Bone #	Length (mm)	Mass (g)	CC proximal (mm)	ML proximal (mm)	CC distal (mm)	ML distal (mm)	d_{CC} (mm)	d_{ML} (mm)	Area (mm^2)	Perimeter (mm)
1	365	1038	111	81	81	53	44	32	1101	243
2	345	1054	108	77	83	48	48	34	1206	261
3	316	894	102	78	74	47	43	28	965	228
4	368	1610	122	92	97	54	57	42	1777	315
5	400	1504	117	87	88	55	55	36	1605	292
6	405	1408	113	80	79	50	47	33	1298	255
7	410	1676	118	82	86	58	54	37	1555	291
8	357	1200	109	84	78	45	41	36	1152	242
9	370	1300	105	72	69	47	44	31	1080	240
10	387	1380	120	102	83	62	47	33	1203	254
11	372	1217	117	97	82	58	47	32	1174	252
12	410	1380	114	106	71	51	50	33	1293	266
13	415	1697	127	104	86	61	54	37	1569	290

The data acquisition module NI PXIe-4492 was mounted on NI PXIe-1082 chassis. Data were collected at sampling rate of 8 kHz for duration of 300 milliseconds to ensure that the response is completely damped.

B. Methodology

1. *Frequency Response Function (FRF)*

The response in the FRF can be represented as a displacement, velocity, or acceleration. The FRF $H(\omega)$ (Equation 1) is defined as the Fourier transform of an output response $X(\omega)$ to the Fourier transform of the input force $F(\omega)$ [55].

$$H(\omega) = \frac{X(\omega)}{F(\omega)} \tag{1}$$

The analysis of the frequency response function $H_1(f)$ with random noise and distortion summing up to the output, consists of three main stages. The first stage of the analysis requires the calculation of the cross spectral density of the input and the output which is given by the symbol $S_{xy}(f)$. This calculation is implemented by using the response as the first input and the excitation as the second input. The second stage involves determining the auto spectral density of the input $S_{xx}(f)$. Last, the frequency response function (FRF) is obtained (Equation 2), which is the ratio of the cross-spectral density $S_{xy}(f)$ to the auto spectral density $S_{xx}(f)$) [55].

$$H_1(f) = \frac{S_{xy}(f)}{S_{xx}(f)} \tag{2}$$

where,

$S_{xx}(f)$: Auto spectral density of the output and input

$S_{xy}(f)$: Cross spectral density of the input

Similarly, if random noise and distortion are summed up to the input, the frequency response function $H_2(f)$ becomes defined by:

$$H_2(f) = \frac{S_{yy}(f)}{S_{yx}(f)} \tag{3}$$

Where,

$S_{yy}(f)$: Auto spectral density of the output

$S_{yx}(f)$: Cross spectral density of the output and input

Measured responses in time domain were transformed to frequency domain using Fast Fourier Transform (FFT) algorithm. The FRF was then found using the noise-free FRF formulation given by Equation 1, considering that the damping table and excised bone reduced random noise to some extent. Later, the resonant frequencies were determined by manual peak picking. A representative FRF spectrum (for Bone 6) based on the four accelerometers response and impact at location 2 is shown in Figure 3.

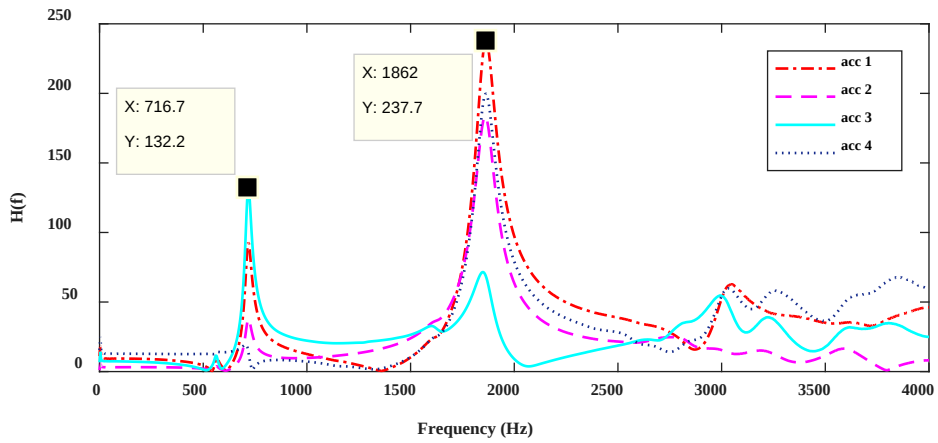

Figure 3. Sample frequency response plots for Bone 6 generated using the data from the four accelerometers – lateral direction; acc: accelerometer.

2. *Complex Mode Indicator Function (CMIF)*

CMIF is a practical procedure that necessitates minimal user intervention to produce modal frequencies. It is characterized by the eigenvalues and solved from the normal FRF matrix at each spectral line. The normal matrix can be obtained by post-multiplying the FRF matrix by its Hermitian Matrix $[H(\omega)][H(\omega)]^H$ [56].

$$[H] = [U][S][V]^H \tag{4}$$

$$[H(\omega)]^H[H(\omega)] = [V(\omega)]\,[\Lambda(\omega)][V(\omega)]^H \tag{5}$$

A more precise representation of the above equations is given by:

$$[H]_{N_0\times N_i}[H]^H_{N_0\times N_i} = [V]_{N_0\times N_i}[\Lambda]_{N_0\times N_i}[V]^H_{N_0\times N_i} \tag{6}$$

$$CMIF_k(\omega) = \mu_k = s_k(\omega)^2 . k = 1,2,\ldots N_i \tag{7}$$

Where,

$[H]$: FRF matrix

$[\,]^H$: Hermitian (conjugate transpose) of a matrix

$[U]$: Left singular matrix, corresponding to matrix of the mode shape vectors

$[S]$: Diagonal singular value matrix

$[V]$: Right singular matrix, corresponding to the matrix of modal participation vector

$[\Lambda]$: Diagonal eigenvalue matrix

$CMIF_k(\omega)$: k^{th} CMIF at frequency ω

$\mu_k(\omega)$: k^{th} Eigenvalue of the normal matrix at frequency ω

$s_k(\omega)$: k^{th} Singular value of the FRF matrix at frequency ω

N_i : Number of inputs

N_0 : Number of outputs

The procedure to obtain CMIF plots is illustrated in Figure 4. Eigenvalues are solved using the preceding equations and later plotted as magnitude (or log magnitude) scale against frequency. Local maxima or minima are observed indicating the presence of physical modes. Frequency values of observed peaks are the natural damped frequencies of each mode. The formulation was implemented in custom MATLAB code to compute and plot the CMIF spectrum. EMA data that includes hammer impact (input) and response from 4 accelerometers (output) were loaded into the code and numerical calculations were implemented. The code accepts the input and data from each accelerometer simultaneously, builds and solves the matrix systems to find the eigenvalues, and plots values with respect to frequency.

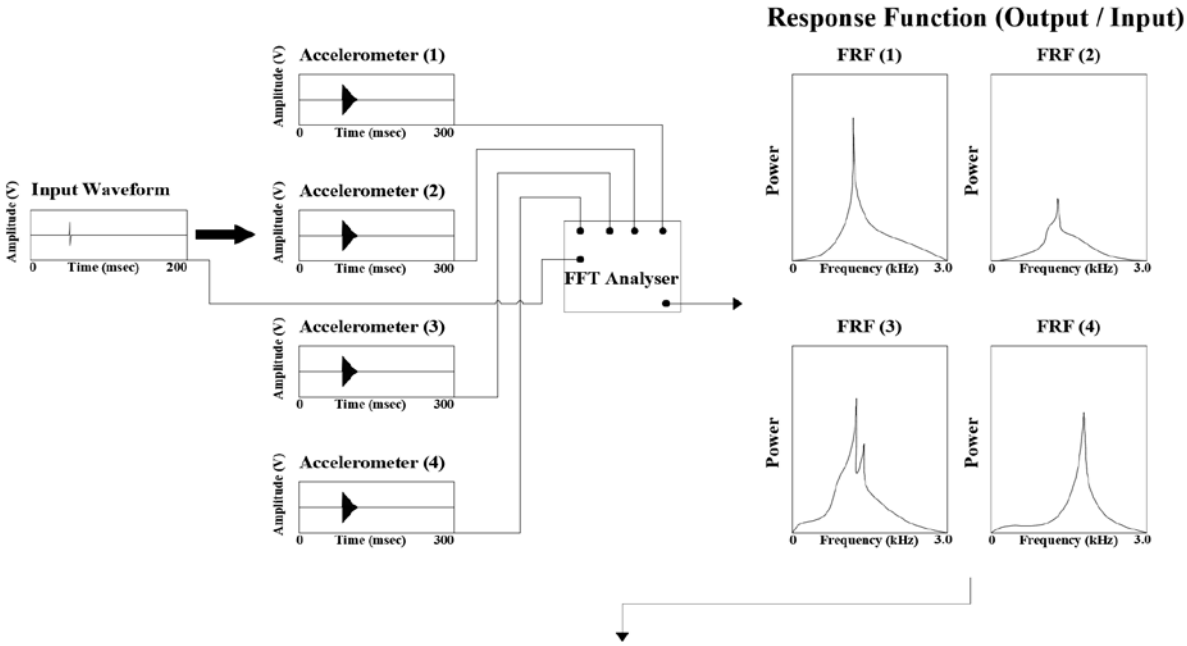

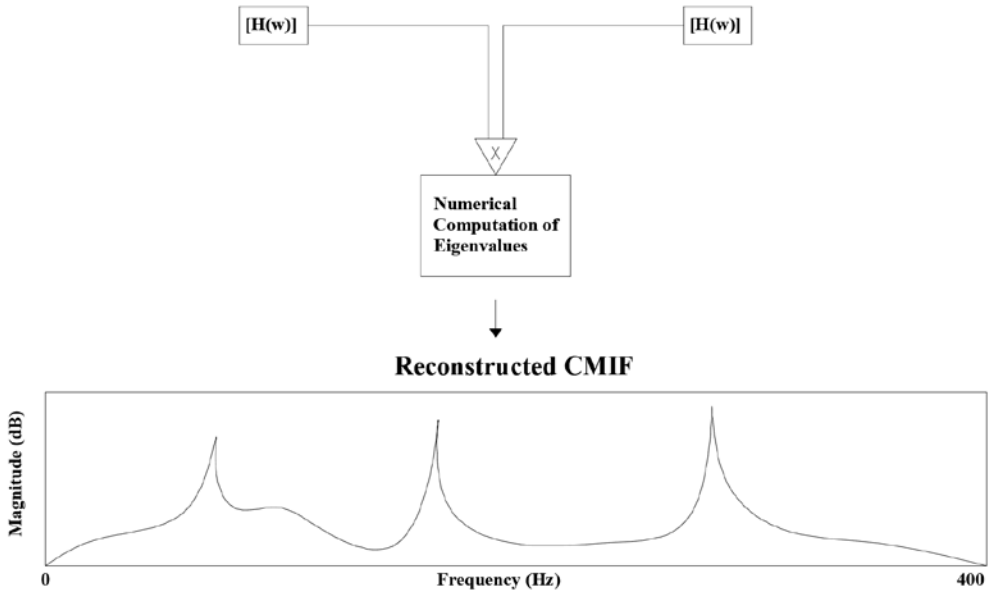

Figure 4. Schematic of the analysis procedure based on the CMIF.

CHAPTER IV

NUMERICAL WORK

A. FEM Model Preparation

1. *Bone Segmentation from CT Scans*

For model preprocessing to ANSYS, CT scans (Philips Brilliance iCT scanner) were obtained for tibia bones collected from the hind legs of a 2-year-old cow (dubbed Bone A): slice thickness of 0.67 mm and spacing of 0.33 mm and resulting in voxel size of 0.32 mm. Total number of 1255 slices were passed to Mimics in DICOM format where segmentation was performed using threshold values chosen for compact or cancellous bone tissue. Figure 5 displays CT scans where top left, top right, and bottom left images depict the medial-lateral, axial, and cranial-caudal planes, respectively.

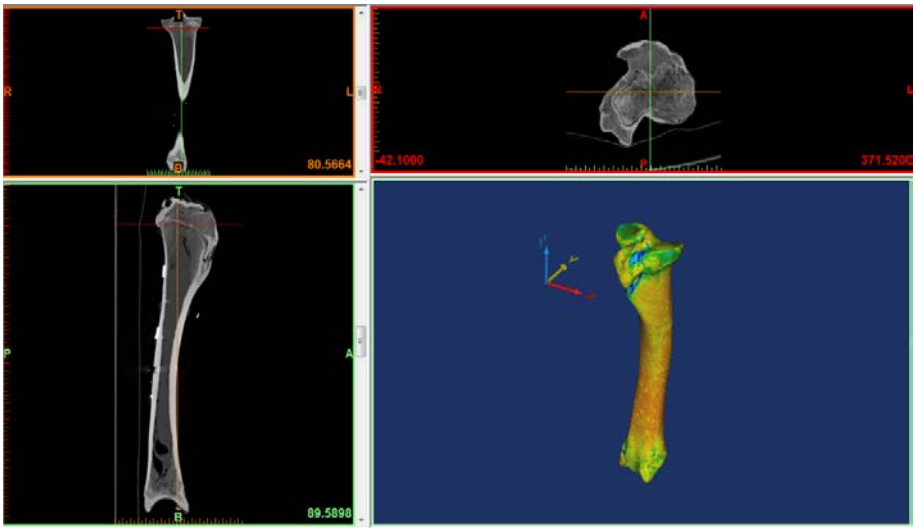

Figure 5. CT scans in different planes; top left: medial-lateral plane (x-z axis), top right: axial plane, bottom left: cranial-caudal plane (y-z axis); bottom right: 3D model.

2. *FEM Model*

Following segmentation and in preparation for element meshing, the 3D bone model is processed using 3matic (also from Materialize) for surface and volume meshing (for more details see [57]). A free-free boundary condition is considered in ANSYS to mimic the boundary conditions imposed in the experimental dynamic assessment conducted by Hamade and coworkers [23]. In addition to bone tissue, the CT scans also captured the mounting hardware needed to attach the piezoelectric sensors needed in the experiments. The meshed 3D model for Bone A consisted of 473704 linear tetrahedral (Tet 4) elements and 83890 nodes.

B. Material Assignment

1. *Stiffness-Density Formulae*

In relating stiffness to apparent density of cortical and cancellous bone tissue, both power and linear form relations are reported in the literature. A summary of the literature-surveyed equations along with relevant attributes is listed in Table 2. Co-listed are equations suggested by Mimics [21]. Table 2 lists various anatomical attributes studied as well as testing protocol details that help put the considered formulae in context.

Table 2 also lists apparent density ranges and corresponding ranges of the modulus of elasticity. Listed are seven cortical (compact) formulae, four cancellous formulae, and three formulae applicable to both constituents (that of [43]). Employing 25 cancellous and 2 cortical data points for a scapula (flat bone having less cortical tissues than long bones), Gupta and Dan [43] proposed the only formulae applicable to

both cortical and cancellous bone constituents. The maximum modulus value (starting from zero modulus) calculated was $E = 22.8$ GPa (at $\rho = 1.8 \frac{g}{cm^3}$). They specified two ranges of stiffness for cancellous cell structures: one for open ($0 < E < 0.13$ GPa for $0 < \rho < 0.35 \frac{g}{cm^3}$) and another for closed ($0.13 < E < 17.5$ GPa for $0.35 < \rho < 1.8 \frac{g}{cm^3}$). Snyder and Schneider [40] considered modulus range ($13.74 < E < 20.32$ GPa) for cortical tibia bone with axial stiffness of $E = 17.3$ GPa (for $\rho = 1.861 \frac{g}{cm^3}$) with examined density range of $1.7 < \rho < 2 \frac{g}{cm^3}$. Linear and power relations were studied in the corresponding reference.

Lotz et al. [41] developed cortical equation for femur long bone obtained from specimens collected mainly from metaphyseal region (relatively thin cortex shell). Formulae yield relatively low stiffness values in the range $5.82 < E < 14.38$ GPa for density range $1.35 < \rho < 1.95 \frac{g}{cm^3}$ with one sample calculation yielding $E = 12.23$ GPa at $\rho = 1.8 \frac{g}{cm^3}$.

Wirtz et al. [44] developed a cortical equation by considering two experimentally based literature studies [41, 45]. Formula estimates stiffness value for $E = 12.67$ GPa (at $\rho = 1.8 \frac{g}{cm^3}$) and $E = 21$ GPa (at $\rho = 1.85 \frac{g}{cm^3}$) and modulus range of $7.22 < E < 20.14$ GPa (for $1.5 < \rho < 2.09 \frac{g}{cm^3}$) and $13.74 < E < 23.6$ GPa (for $0.2 < \rho < 2 \frac{g}{cm^3}$), respectively.

The cortical investigation by Austman et al. [46] was based on ulna (long bone) with 8 extracted specimens from the distal region that may have contained more trabecular bone (cancellous bone with high material properties) than cortical given that it came from the lower metaphyseal part of the bone. In the longitudinal direction,

average compressive modulus for human cortical bone is estimated at about $21\ \mathrm{GPa}$ [9, 58-60]. Note that the MIMICS recommended $\mathrm{E} - \rho$ relation for cancellous bone does not cite basis for their recommendation. Relating to cancellous bovine bone with relatively low densities ($0.2 < \rho < 0.7\ \frac{\mathrm{g}}{\mathrm{cm}^3}$), a formula proposed by Keaveny et al. [42] yielded stiffness modulus values in the range $0.7 < E < 3.744\ \mathrm{GPa}$. While, for cortical bovine bone Huang et al. [51] estimated stiffness values of $\mathrm{E} = 11.47\ \mathrm{GPa}$ at $\rho = 1.8\ \frac{\mathrm{g}}{\mathrm{cm}^3}$. For bovine cortical bone at mid diaphysis of long bones, values of about $20\ \mathrm{GPa}$ have been reported [57, 61-64].

Table 2. Description of formulae considered in this work.

Refs	Type of bone			Region studied	Sample tested	Age (years)	# of samples	Orientation	Geometrical dimensions b x w x t or d x l (mm)	Range of tested apparent density ($\frac{\mathrm{g}}{\mathrm{cm}^3}$) / modulus of elasticity (GPa)
[40]	Human	Long bone - tibia	Cortical	Mid-diaphysis	Flat rectangular plate	29-73	45 specimens	longitudinal	2x2x40	$1.7 < \rho_{app} < 2.0$
										$13.74 < E < 20.32$
[41]	Human	Long bone - femur	Cortical	Metaphyseal	Flat rectangular prismatic plate	28-90	123 specimens	longitudinal	7x5x0.4	$1.35 < \rho_{app} < 1.95$
				Diaphyseal			36 specimens			$5.82 < E < 14.38$
[42]	Bovine	Long bone - tibia	Cancellous	Proximal	Flat rectangular plate	NA	38 specimens	longitudinal	3x3x1	$0.2 < \rho_{app} < 0.7$
										$0.7 < E < 3.744$
[43]	Human	Flat bone - Scapula (glenoid)	Cortical	Subchondral	Flat rectangular plate	NA	25 cancellous points	longitudinal	6.5x8	$0 < \rho_{app} < 2.0$
							2 cortical			$0 < E < 22.8$

							points			
[43]	Human	Flat bone - Scapula (glenoid)	Cancellous	Subchondral	Flat rectangular plate	NA	25 cancellous points	longitudinal	6.5x8	$0 < \rho_{app} < 0.35$ & $0.35 < \rho_{app} < 1.8$ $0 < E < 0.13$ & $0.13 < E < 17.5$
[44]	[41] + [45]									
[45]	Human	Long bone - tibia	Cortical	Diaphyseal	Flat rectangular plate	16-55	51 specimens	longitudinal	NA	$1.6 < \rho_{app} < 2.1$ $8 < E < 21$
[46]	Human	Long bone - ulna	Cortical	Distal	Flat rectangular plate	60-76	8 specimens	longitudinal	NR	$0.2 < \rho_{app} < 2.0$ $13.74 < E < 23.6$
[51]	Bovine	Long bone - femur	Cortical	Diaphyseal	Cubic specimen	NA	10 specimens	longitudinal	10x10x10	NA NA
[21]	NA	Long bone - tibia	Cortical, Cancellous	Proximal	NA	NA	NA	longitudinal	NA	NA NA

For potentially accurate material assignment for cortical and cancellous constituents, Table 3 lists 22 cases of stiffness vs. density literature-reported formulae. All E-density relations were modified to fit units of E: MPa and density: $\frac{\text{tonnes}}{\text{mm}^3}$. These cases constitute single formula or combinations of the formulae listed in Table 2. Apparent is the immense variety of formulation between linear and power yielding, for same bone density, great differences were seen in estimated weighted average E values (Section *Weighted average modulus of elasticity* below).

Table 3. Twenty two different cases considered (cancellous-1, -2, and -3 refer to different formulae in Table 1). Units: E: MPa and density: $\frac{\text{tonnes}}{\text{mm}^3}$

Case #	Formulae	References	Weighted average modulus of Elasticity (MPa)
Case 1	$E = 5.901975 * 10^{31} * \rho_{app}{}^{3.15}$ (compact & cancellous-1)	[43]	13888.88
Case 2	$E = 5.288 * 10^{21} * \rho_{app}{}^{2}$ (compact & cancellous-2)	[43]	14655.61
Case 3	$E = 2.998 * 10^{30} * \rho_{app}{}^{3}$(compact & cancellous-3)	[43]	14482.69
Case 4	$E = 1.3 * 10^{13} * \rho_{app} - 3842$ (compact) $E = 1.04925 * 10^{21} * \rho_{app}{}^{2}$ (cancellous: $\rho \leq 0.35$) $E = 3 * 10^{30} * \rho_{app}{}^{3}$ (cancellous: $0.35 \leq \rho \leq 1.8$)	[21] [43] [43]	14947.71
Case 5	$E = 2.63923694 * 10^{17} * \rho_{app}{}^{1.5}$ (compact) $E = 1.04925 * 10^{21} * \rho_{app}{}^{2}$ (cancellous: $\rho \leq 0.35$) $E = 3 * 10^{30} * \rho_{app}{}^{3}$ (cancellous: $0.35 \leq \rho \leq 1.8$)	[46] [43] [43]	15356.47
Case 6	$E = -13430 + (1.4261 * 10^{13} * \rho_{app})$ (compact) $E = 1.04925 * 10^{21} * \rho_{app}{}^{2}$ (cancellous: $\rho \leq 0.35$) $E = 3 * 10^{30} * \rho_{app}{}^{3}$ (cancellous: $0.35 \leq \rho \leq 1.8$)	[41] [43] [43]	10924.28
Case 7	$E = 1.3 * 10^{13} * \rho_{app} - 3842$ (compact) $E = 1.221905 * 10^{15} * \rho_{app}{}^{1.33}$ (cancellous-1)	[21] [21]	12462.06
Case 8	$E = 2.63923694 * 10^{17} * \rho_{app}{}^{1.5}$ (compact) $E = 2.94297925 * 10^{16} * \rho_{app}{}^{1.46}$ (cancellous-2)	[46] [21]	13521.35
Case 9	$E = -2.35 * 10^{4} + (2.191 * 10^{13}) * \rho_{app}$ $E = 1.04925 * 10^{21} * \rho_{app}{}^{2}$ (cancellous: $\rho \leq 0.35$) $E = 3 * 10^{30} * \rho_{app}{}^{3}$ (cancellous: $0.35 \leq \rho \leq 1.8$)	[40] [43] [43]	13251.91
Case 10	$E = 1.3 * 10^{13} * \rho_{app} - 3842$ (compact) $E = 2.94297925 * 10^{16} * \rho_{app}{}^{1.46}$ (cancellous-2)	[21] [21]	13027.97
Case 11	$E = -13430 + (1.4261 * 10^{13} * \rho_{app})$ (compact) $E = 1.221905 * 10^{15} * \rho_{app}{}^{1.33}$ (cancellous-1)	[41] [21]	8523.24
Case 12	$E = -2.35 * 10^{4} + (2.191 * 10^{13}) * \rho_{app}$ $E = 1.221905 * 10^{15} * \rho_{app}{}^{1.33}$ (cancellous-1)	[40] [21]	10850.87
Case 13	$E = 2.63923694 * 10^{17} * \rho_{app}{}^{1.5}$ (compact) 3. $E = 1.221905 * 10^{15} * \rho_{app}{}^{1.33}$ (cancellous-1)	[46] [21]	12955.43
Case 14	$E = -13430 + (1.4261 * 10^{13} * \rho_{app})$ (compact) 4. $E = 2.94297925 * 10^{16} * \rho_{app}{}^{1.46}$ (cancellous-2)	[41] [21]	9089.143
Case 15	$E = -2.35 * 10^{4} + (2.191 * 10^{13}) * \rho_{app}$ $E = 2.94297925 * 10^{16} * \rho_{app}{}^{1.46}$ (cancellous-2)	[40] [21]	11416.78
Case 16	$E = 1.33327598 * 10^{31} * \rho_{app}{}^{3.09}$ (compact) $E = 1.04925 * 10^{21} * \rho_{app}{}^{2}$ (cancellous: $\rho \leq 0.35$) $E = 3 * 10^{30} * \rho_{app}{}^{3}$ (cancellous: $0.35 \leq \rho \leq 1.8$)	[44] [43] [43]	11555.33
Case 17	$E = 1.33327598 * 10^{31} * \rho_{app}{}^{3.09}$ (compact) $E = 1.221905 * 10^{15} * \rho_{app}{}^{1.33}$ (cancellous-1)	[44] [21]	9154.309
Case 18	$E = 1.33327598 * 10^{31} * \rho_{app}{}^{3.09}$ (compact)	[44] [21]	9720.212

	$E = 2.94297925 * 10^{16} * \rho_{app}{}^{1.46}$ (cancellous-2)		
Case 19	$E = 8.62552 * 10^{20} * \rho_{app}{}^{1.93}$ (compact) $E = 6510 * \rho_{app} - 813$ (cancellous)	[51] [42]	10541.75
Case 20	$E = 1.259102919 * 10^{25} * \rho_{app}{}^{2.39}$ (compact) $E = 2.94297925 * 10^{16} * \rho_{app}{}^{1.46}$ (cancellous-2)	[40] [21]	11383.29
Case 21	$E = 1.259102919 * 10^{25} * \rho_{app}{}^{2.39}$ (compact) $E = 1.221905 * 10^{15} * \rho_{app}{}^{1.33}$ (cancellous-1)	[40] [21]	10817.6308
Case 22	$E = 1.259102919 * 10^{25} * \rho_{app}{}^{2.39}$ (compact) $E = 1.04925 * 10^{21} * \rho_{app}{}^{2}$ (cancellous: $\rho \leq 0.35$) $E = 3 * 10^{30} * \rho_{app}{}^{3}$ (cancellous: $0.35 \leq \rho \leq 1.8$)	[40] [43] [43]	13216.94

2. *Method of Material Assignment*

The tibia bone is transferred from 3-matic back to Mimics for material assignment according to gray value whereby cancellous and cortical constituents are demarcated according to HU values that define material apparent density. The cut-off value to demarcate these two types of materials is arrived at by developing a method to accurately estimate the measured bone mass of Bone A. Cut-off HU and density values were reached at by developing their varying response to the change of weighted average density (i.e. bone mass). Two linear relations are formulated with respect to the mass, and then the cut-off HU and the cut-off density values were set for values that satisfy the measured mass for Bone A. The study was done on a range of HU and density values. A range of density between 1.6 and 1.8 $\frac{g}{cm^3}$, displayed an increasing effect of the cut-off density on the bone mass (Figure 6(a)). For a mass of 1.408 kg, the cut-off density was approximated to **1.7455** $\frac{g}{cm^3}$. Figure 6(b) shows that the bone mass decreases as the cut-off HU value increase, since the number of cortical bone elements will decrease. For a mass of 1.408 kg the cut-off HU value was equal to **500**. The total number of materials used was examined for their effect on the bone mass. The bone

mass varies as increasing the number of materials (Figure 6(c)), until it reaches a steady-state where the number of assigned materials will no longer be influential (for number of materials >**156**).

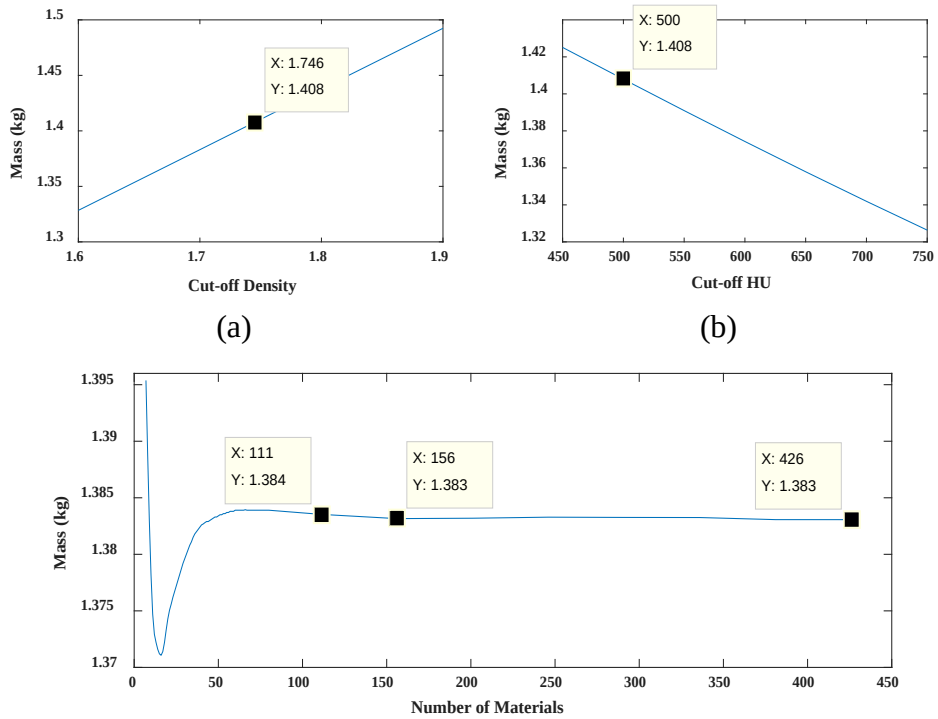

Figure 6. (a) Bone mass (kg) versus cut-off density ($\frac{g}{cm^3}$), **(**b) bone mass versus cut-off HU, (c) average density versus number of materials.

The values of the variables used are 426 as the number of materials, 500 as the cut-off HU value and 1.7455 $\frac{g}{cm^3}$ as the cut-off density value. To differentiate regions of very low density from those of higher densities, cancellous bone was split into two sub-constituents over 2 HU intervals. The range of the least dense cancellous bone [13] extends from the lowest value of -1024 HU (density near $0\frac{g}{cm^3}$) to HU = -710 (density of $0.35\frac{g}{cm^3}$). This is illustrated in Figure 7(a) which is a histogram plot of number of elements assigned for each material with respect to HU where the elements on the very left represent bone of very low density and stiffness with negative CT numbers. The

next denser cancellous material in Figure 3(a) has HU extending over the range of HU = -710 to 499 HU ($1.7455\frac{g}{cm^3}$ density). Further to the right are cortical bone elements with up to maximum cortical density of $\rho = 2.07\frac{g}{cm^3}$ [62]. Literature works related material properties by power laws while maintaining one parameter as constant (e.g. Poisson's ratio) [65]. The Poisson's ratio was considered as homogeneous and equal to $\upsilon = 0.3$ [44]. The elements on the extreme right (HU >2896) represent materials of foreign nature (ceramic piezoelectric sensors) on bone surface ($\rho = 6\frac{g}{cm^3}$,$\upsilon = 0.3, E = 200$ GPa). Elemental distribution of bone materials is shown pictorially in Figure 7(b). Note the additional ceramic hardware are needed for dynamic testing (highest HU values). The variation of colors from blue to red represent the range of HU values per Figure 7(a) from the lowest HU value to the highest. The cortical shell in mid-diaphysis region has the highest stiffness value (in turns it has the highest HU value), however it does not show "dark red" region, since the color variation is varied along the bone marrow (very low stiffness value) and the ceramic plates (E=200 GPa). Hence, according to this interval ~21GPa which is the cortical stiffness is not the highest.

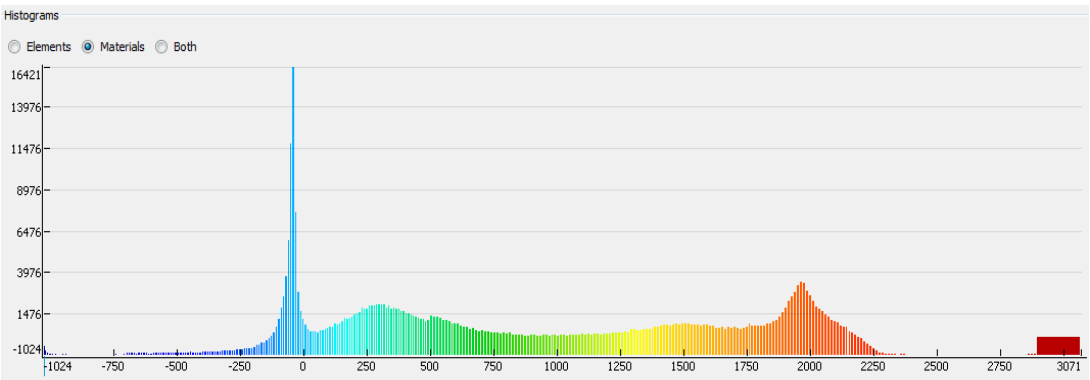

(a)

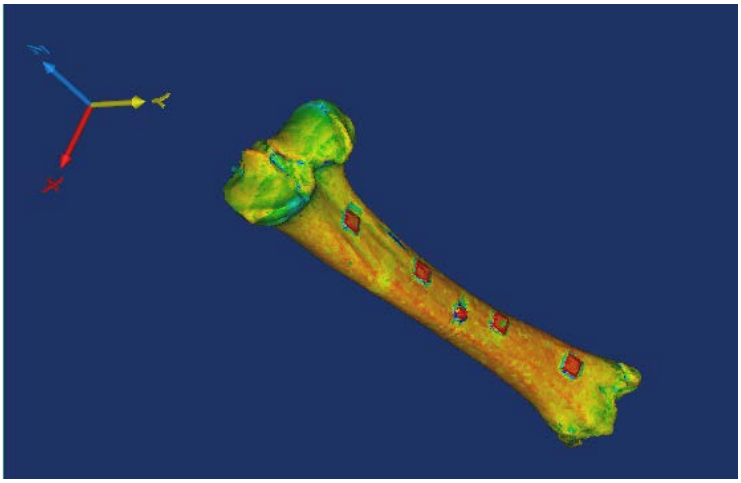

(b)

Figure 7. (a) Number of elements vs. HU range, (b) bone with materials' properties assigned for the meshed elements.

3. *Weighted Average Modulus of Elasticity*

Based on the HU cutoff values above for Bone A, the FEM model yielded weighted average density value of $\rho = 1.6027\,\frac{\mathrm{g}}{\mathrm{cm}^3}$ and total mass of $m = 1.402\ \mathrm{kg}$ (0.42 % difference from the measured mass). The weighted average modulus of elasticity for each case in Table 4 (last column) differ depending on the equations used (last column in Table 3) calculated relative to total number of elements according to Equations (8) and (9).

Weighted average value of density:

$$\rho_{avg} = \frac{\sum N.\rho_N}{N_T} \tag{8}$$

Weighted average value of modulus of elasticity:

$$E_{avg} = \frac{\sum N.E_N}{N_T} \tag{9}$$

Where, *N*: Number of elements

ρ: Apparent density

E: Modulus of elasticity

N_T: Total number of elements

4. *Distinctions of Current Work with Other Work Reported in the Literature*

This work is compared to studies reported by Taylor et al. [7] and Scholz et al. [9]. Table 4 lists differences between this work and previous works. Taylor et al. [7] estimated modal frequencies of a cadaveric femur using CT scans and finite element analysis for numerical approach. Material constants as bone mass, elastic constants were estimated by fitting the orthotropic numerical data to the measured values. Their objective was to investigate if modal analysis would predict the bone's material constant. The material properties were varied so that the first computed natural frequencies (numerically and experimentally) are equal. All bone materials had the same density-HU quadratic relation, and only 42 different material groups were created for bone constituents. Scholz et al. [7] examined the suitability of three literature density-elasticity relations [8, 9, 11] for human pelvic bone that were formulated from long bones in previous works. The bones were CT scanned, and then segmented and processed in MIMICS. The model mass was adjusted to approach the measured mass value of the referenced work using a series that should have the least value upon getting the difference between masses.

Table 4. Comparison of this work and previous works Taylor et al [7] and Scholz et al. [9].

References / Differences	Taylor et al [7]	Scholz et al. [9]	This work
Test type	Modal analysis	Modal analysis	Modal analysis
Specimen type	Human femur	Human pelvic	Bovine tibia
Scope	The study focuses on matching numerical and experimental results for the first natural frequency solely, by modifying the material constants.	The study examined the suitability of three literature density-elasticity relations for human pelvic bone that were formulated from long bones in previous works.	The study focuses on assessing the most suitable stiffness-density combination among all what was found from the literature using the apparent density.
Model mass	Model mass is modified to match the measured value, by varying the moduli values.	Model mass was adjusted to approach the measured mass value.	Model mass was reached for upon varying the cut-off point and the number of materials. The cut-off point is the point separating bone constituents.
Material assignment	All bone materials had the same density-HU quadratic relation.	The stiffness-density relationships were assumed valid for cancellous and cortical bone constituents.	Different bone constituents were assigned different stiffness-density relationships, depending on the formulating process.
Material Properties	Bone is orthotropic.	Bone is isotropic.	Bone is isotropic
Stiffness relation	Stiffness values did not vary with the apparent density.	Stiffness depends on the apparent and ash density	Stiffness depends on the apparent density
Number of materials	Small number of materials were set for the cancellous bone HU region.	–	The number of materials of cancellous and cortical bones were close and high with a total of 426 for both.
Density-stiffness relationships	–	Three different literature density-stiffness relationships were examined; three: cortical + cancellous.	13 different literature density-stiffness relationships were examined; six: cortical, four: cancellous and three: cortical + cancellous.
Case combination	–	No cases were examined	19 cases were created from these eight relationships for cancellous and cortical bones.
Test examination	–	No retesting was done	Retested on a new bone

CHAPTER V

RESULTS AND DISCUSSION

A. FRF vs. CMIF

1. *Modal Frequencies*

a. Cranial-Caudal Modal Frequencies: FRF and CMIF Methods

Based on FRF data resulting from an average of 10 impacts at the same location, the first and second modes are captured. Sample FRF reconstructed CMIF plots of magnitude vs. frequency are plotted in Figure 8 (A). Also plotted frequency plots at 3 locations are shown in Figure 8 (B-D). The frequencies of each of the modes were reported from each accelerometer and for every impact location but only average values and standard deviation values are listed in Table 5. The first modal frequency captured for each of the bones was consistent across the four accelerometers used and for the same impact location. For instance, based on the four accelerometer readings the first bending mode of Bone 6 was determined to be 516.5 Hz. This slightly differed between individual accelerometers with a maximum difference of 1 Hz. The percentage difference was larger when the second mode was considered (reaching 23 Hz). Some variations were observed in frequency values reaching 1.63% when changing impact location. The second bending mode frequency (e.g. 1458.5 Hz for Bone 6) values varied depending on the measurement location, as well as the impact location, resulting in variation of 12.44%.

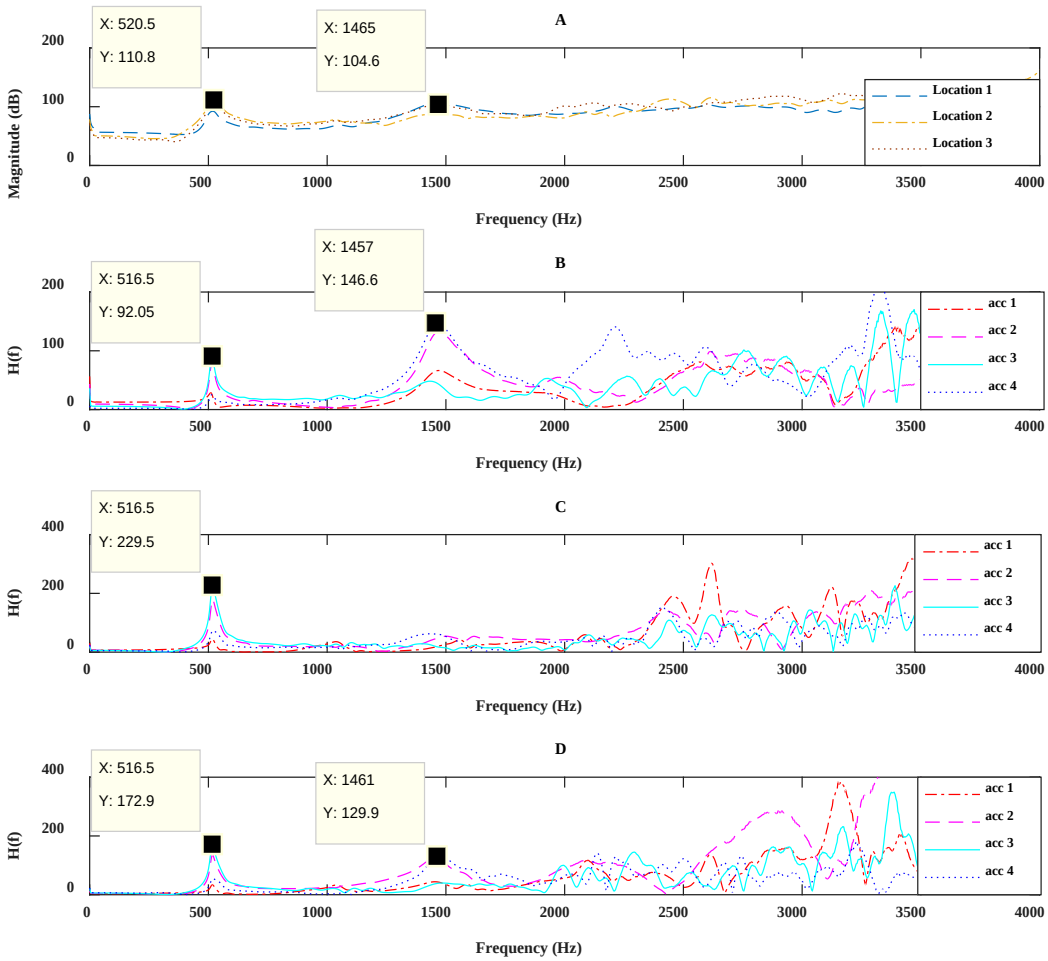

Figure 8. Sample CMIF plots vs. FRF at different impact locations for Bone 6 generated using the data from each accelerometer – Cranial-Caudal Direction; Reconstructed CMIF (A); Frequency response function- (B) Location 1; (C) Location 2; (D) Location 3.

Raw data were processed using the CMIF to extract the first and second bending mode. The first bending mode for Bone 6 was determined to be 520.5 Hz, while the second mode was found to be 1465 Hz (example is shown in Figure 8 (A)). The influence of the impact location on the measured frequency was less significant with the CMIF technique, with a maximum variation of 1.63% and 6.27%, for the first and second mode respectively. Variation in the geometrical differences and mass variations amongst all bones gave rise to difference in the modal frequencies calculated.

Table 5. Average (and Std dev) values of resonant frequencies (Hz) obtained from FRF method and CMIF – Cranial-Caudal plane.

			Location 1		Location 2		Location 3		average values	
			Mode 1	Mode 2	Mode 1	Mode 2	Mode 1	Mode 2	Mode 1	Mode 2
Bone 1	FRF	Average (stdev)	597 (0)	1605 (29)	596 (2)	*	596 (2)	1590 (0)	596	1598
	CMIF		601	1586	601	1582	601	1582	601	1583
Bone 2	FRF	Average (stdev)	661 (0)	2352 (15)	665 (0)	2458 (13)	654 (10)	2467 (12)	660	2426
	CMIF		665	2358	665	*	672	2342	667	2350
Bone 3	FRF	Average (stdev)	697 (6)	1797 (24)	696 (10)	1771 (12)	704 (6)	1991 (80)	699	1853
	CMIF		705	1822	701	1802	705	1854	703	1826
Bone 4	FRF	Average (stdev)	742 (2)	1465 (28)	743 (2)	1502 (0)	744 (6)	1445 (0)	743	1471
	CMIF		741	1481	749	1502	753	1574	747	1519
Bone 5	FRF	Average (stdev)	628 (2)	1686 (18)	628 (2)	1681 (20)	625 (3)	1669 (23)	627	1679
	CMIF		629	1686	629	1686	633	1682	630	1685
Bone 6	FRF	Average (stdev)	514 (1)	1456 (15)	521 (0)	*	517 (0)	1461 (0)	517	1459
	CMIF		521	1465	521	1465	521	1465	521	1465
Bone 7	FRF	Average (stdev)	627 (2)	1248 (13)	629 (0)	1251 (2)	629 (0)	1251 (2)	628	1250
	CMIF		625	1249	625	1249	625	1249	625	1249
Bone 8	FRF	Average (stdev)	765 (3)	2183 (12)	765 (3)	2186 (10)	765 (3)	2185 (8)	765	2185
	CMIF		773	2178	773	2178	773	2178	773	2178
Bone 9	FRF	Average (stdev)	588 (2)	2148 (34)	588 (2)	2146 (22)	589 (0)	2149 (33)	588	2148
	CMIF		585	2130	585	2130	585	2130	585	2130
Bone 10	FRF	Average (stdev)	530 (2)	1640 (70)	526 (2)	1686 (97)	527 (4)	1529 (43)	527	1618
	CMIF		529	1658	529	1686	529	1682	529	1675
Bone 11	FRF	Average (stdev)	564 (6)	1515 (104)	557 (0)	*	559 (2)	1490 (28)	1502	2008
	CMIF		557	1461	566	1461	557	1465	1462	2038
Bone 12	FRF	Average (stdev)	595 (4)	1595 (15)	594 (2)	*	594 (2)	1608 (66)	594	1602
	CMIF		593	1598	593	1594	593	1598	593	1597
Bone 13	FRF	Average (stdev)	584 (6)	1612 (26)	582 (2)	*	582 (2)	1608 (40)	582	1610
	CMIF		581	1618	581	1622	581	1626	581	1622

[*] *Frequency mode was not captured*

b. Medial-Lateral Modal Frequencies: FRF and CMIF Methods

Based on FRF data resulting from an average of 10 impacts at the same location (Figure 9 (B-D), the first and the second modes were captured in the Medial-

Lateral direction. The frequencies of each of the modes were recorded from each accelerometer and for every impact location. The first modal frequency captured for each of the bones was more consistent than the second modal frequency captured across the four accelerometers used and for the same impact location. For example, the first bending mode of Bone 6 at location 1 was determined to be 714 Hz on average (based on four accelerometer readings) where the maximum difference between the average value and a reported value from the accelerometers was determined to be 9 Hz. On the other hand, for the second modal frequency captured at location 1 for Bone 6, the maximum difference between the average value of the second modal frequency (1859 Hz) and a reported value from the accelerometers was 13 Hz. Some variation was observed in the first modal frequency value (e.g. 714 Hz for Bone 6) reaching 2.32% when shifting the impact location. The second bending mode frequency (e.g. 1859 Hz for Bone 6) varied within 9.87% depending on the measurement and impact location. Raw data were processed using CMIF to extract the first and second bending modes. The first bending mode for Bone 6 was determined to be 721 Hz, while the second mode was found to be 1865 Hz (an example is shown in Figure 9 (A)). The influence of the impact location on the measured frequency was less significant with the CMIF technique, with a maximum variation of 1.88% and 5.07%, for the first and second modes, respectively.

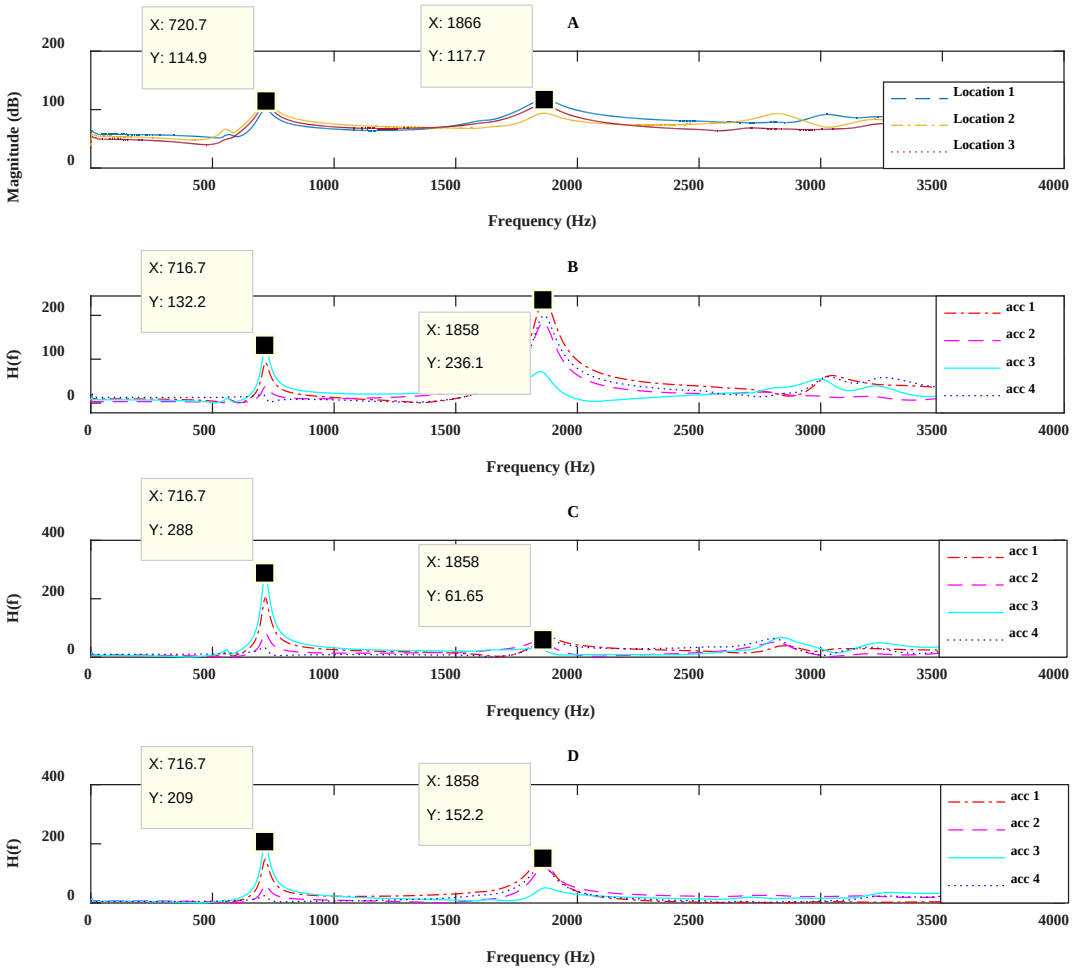

Figure 9. Sample CMIF plots vs. FRF at different impact locations for Bone 6 generated using the data from each accelerometer – Medial-Lateral Direction; Reconstructed CMIF (A); Frequency response function- (B) Location 1; (C) Location 2; (D) Location 3.

Table 6. Average (and Std dev) values of resonant frequencies (Hz) obtained from FRF method and CMIF – Medial-Lateral Direction.

			Location 1		Location 2		Location 3		average values	
			Mode 1	Mode 2	Mode 1	Mode 2	Mode 1	Mode 2	Mode 1	Mode 2
Bone 1	FRF	Average (stdev)	811 (4)	2041 (7)	810 (5)	2045 (21)	807 (7)	2035 (17)	809	2040
	CMIF		813	2042	809	2050	813	2042	811	2045
Bone 2	FRF	Average (stdev)	949 (3)	2201 (6)	951 (2)	2190 (0)	953 (0)	2245 (42)	951	2212
	CMIF		953	2198	949	2186	953	2198	952	2194
Bone 3	FRF	Average (stdev)	1017 (0)	2186 (0)	1012 (18)	*	1016 (10)	2359 (11)	1015	2273
	CMIF		1021	2350	1021	*	1021	2366	1021	2358
Bone 4	FRF	Average	1054	2222	1050	*	1049	2178	1051	2200

		(stdev)	(2)	(8)	(2)		(3)	(56)		
	CMIF		1053	2222	1053	*	1053	2230	1053	2226
Bone 5	FRF	Average (stdev)	865 (8)	2042 (14)	860 (6)	2027 (30)	865 (17)	2030 (22)	863	2033
	CMIF		865	2038	857	2018	861	2038	861	2031
Bone 6	FRF	Average (stdev)	714 (6)	1859 (9)	717 (3)	1856 (16)	717 (3)	1862 (7)	716	1859
	CMIF		721	1866	721	1862	721	1866	721	1865
Bone 7	FRF	Average (stdev)	797 (0)	1969 (20)	797 (0)	1999 (30)	799 (2)	1979 (31)	798	1982
	CMIF		801	1994	801	1994	801	1994	801	1994
Bone 8	FRF	Average (stdev)	941 (6)	2460 (310)	939 (7)	2361 (48)	942 (9)	2310 (20)	941	2377
	CMIF		945	2286	941	2402	945	2314	944	2334
Bone 9	FRF	Average (stdev)	824 (2)	2174 (30)	826 (4)	2223 (14)	830 (17)	*	826	2199
	CMIF		825	2166	825	2218	833	2266	827	2217
Bone 10	FRF	Average (stdev)	649 (9)	2026 (90)	648 (17)	2226 (176)	650 (23)	2174 (0)	649	2142
	CMIF		649	2114	637	2194	641	*	642	2154
Bone 11	FRF	Average (stdev)	753 (20)	2070 (163)	739 (12)	1960 (150)	736 (8)	1995 (119)	742	2008
	CMIF		741	2030	733	*	729	2046	734	2038
Bone 12	FRF	Average (stdev)	809 (29)	1772 (54)	793 (0)	1762 (62)	794 (2)	1772 (62)	799	1769
	CMIF		797	1786	793	*	793	1774	794	1780
Bone 13	FRF	Average (stdev)	747 (4)	2020 (47)	746 (2)	*	746 (2)	2051 (58)	746	2036
	CMIF		749	2034	745	2042	749	2046	747	2041

* *Frequency mode was not captured*

There were few discrepancies in FRF data between the measurement points considered in this study requiring user expertise to identify faulty modal frequencies. CMIF represents a robust data analysis approach due to its capability of dealing with data contaminated with noise and distortion. CMIF can identify the number of modes of a system and the existence of close and repeated roots. Data over several spectral lines can be encountered in the Singular Value Decomposition which decouples orthogonal vectors, yielding into reducing the influence of errors such as data leakage [19].

2. *Mode Shapes*

After the experimental data was acquired, it was processed in ProSig© to compute the FRF data. To generate the corresponding mode shapes, the inverse of the displaced mass at each node (accelerometer) were exported in excel tables and plotted. The mode number is determined by the number of half sine waves that the system admits. The first modes displayed one half wave with a plateau. Two-half sine waves appeared for the second modes. In Figure 10, representative (Bone 6) first and second modes were normalized with respect to the maximum deformation and bone length. The figure shows the actual mode shapes in the (a) Cranial-Caudal and (b) Medial-Lateral planes.

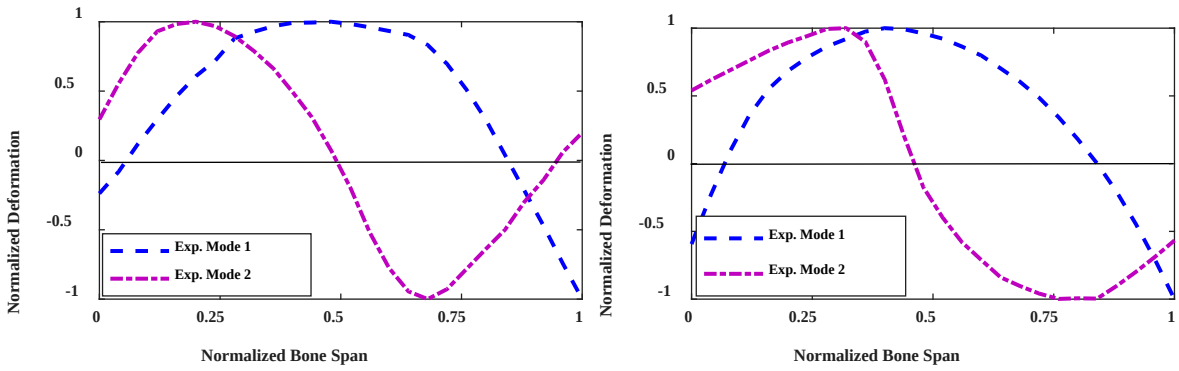

(a) (b)

Figure 10. Experimentally found mode 1 and 2 of tibia Bone 6 in the Cranial-Caudal (a) and Medial-Lateral (b) planes.

B. FEM Results

In this section, FEM modal frequencies estimates will be compared against the results of a dynamic assessment experimental study performed on the same bones by Hamade and co-workers [23]. Experimental measurements for Bone A yielded first and second modal frequencies of 521 Hz and 1465 Hz in the cranial-caudal direction and 721 Hz and 1865 Hz in the medial-lateral plane, respectively.

1. *FEM-Estimated Modal Frequencies*

A free-free system will have the first 6 modes as trivial representing whole body degrees of freedom in the x, y, z, Rx, Ry and Rz directions, so, the first 12 modes had to be computed to reveal the useful first (mode number 7) and second (mode number 10 for cranial-caudal and 11 for medial-lateral) modes.

According to Table 7, the resulting modal frequencies vary greatly throughout the 22 cases due to the equations-combinations listed in Table 3. In case 1, Gupta and Dan [43] equations yielded low frequency values ($F_{n_{case1}} = 89.54$ Hz and $F_{n_{case3}} = 153.62$ Hz). Cases 6, 11 and 14 [41] also computed low frequency values. Cases 16, 17 and 18 based on experimental studies [44] slightly underestimated frequency values. Case 19 based on bovine equations [42, 51] also returned relatively low modal frequencies. This may be since the cancellous equation of Keaveny et al. [42] studied the proximal region (trabecular bones) with low cortical stiffness modulus. The estimates for cases 5, 8 and 13 based on cortical investigation by Austman et al. [43] from an ulna (long bone) came on the high side. Cases 9, 12 and 15 estimated modal frequencies closest to the experimental measurements. These cases employed the cortical equation by Snyder and Schneider [40] but used 3 different cancellous formulae (cancellous -1, -2, and -3). The good estimation power may be due perhaps to the fact that the cortical equation by Snyder and Schneider [40] was attained via employing large number (45) of tibia specimens. However, a power relation from the same literature resulted with low modal frequencies (cases 20, 21 and 22). Both linear and power relations were formulated based on a high correlated data. The affectivity of linear relation is due to a direct linear relation in bone material properties (density and

stiffness), a power relation exaggerates the effect of density on stiffness values for long bones. The age of the examined specimen may also have been consequential, since younger bones are denser and stronger than old ones, thus, having higher stiffness values [64]. In formulating $E - \rho$ relations, specimen geometrical variables play a role as well. Measured stiffness was found to increase with increasing size and aspect ratio of utilized testing specimen [68]. Lotz et al. [41] and Gupta and Dan [43] used low aspect ratio specimens, while Snyder and Schneider [40] used specimens with high aspect ratio.

Table 7. FEM-calculated natural frequencies (Hz) for Bone A.

Case #	Cranial-Caudal Direction		Medial-Lateral Direction	
	1st Mode	2nd Mode	1st Mode	2nd Mode
Case 1	89.54	115.25	99.158	123.78
Case 2	549.46	1731.6	688.92	2018.6
Case 3	153.62	197.01	168.83	213.22
Case 4	563.49	1762.5	704.13	2049.4
Case 5	577.44	1803	722.14	2097.4
Case 6	464.97	1466.3	581.87	1708.6
Case 7	552.18	1689.4	687.89	1952.9
Case 8	570.25	1753.1	711.68	2033.5
Case 9	531.77	1664	666.01	1938.5
Case 10	556.29	1712.9	693.71	1986
Case 11	453.14	1388.7	564.98	1609.9
Case 12	520.17	1586	649.3	1839.4
Case 13	566.15	1726.1	705.84	2000.2
Case 14	457.48	1416	571.09	1643.6
Case 15	524.4	1613.5	655.32	1873.4
Case 16	489.95	1537.5	614.73	1794.1
Case 17	478.08	1458.6	597.65	1693.4
Case 18	482.43	1486.3	603.83	1727.9
Case 19	453.88	1441.1	568.63	1680.9
Case 20	449.22	1425.2	564.02	1656.3
Case 21	435.6	1378.3	546.4	1598.9
Case 22	487.48	1553.3	613.07	1811.6

2. *FEM-Estimated Modal Values and Shapes for Case 12*

FEM-determined mode shapes of first and second natural frequencies in the cranial-caudal and medial-lateral planes employing case 12 are displayed in Figure 11. Larger bone cross-sectional dimensions in the medial-lateral plane will result in higher modal frequency values in that plane compared to that for cranial-caudal plane. First mode is charcterized by two nodes intersecting the deformed and underfomed structure while second mode has 3 nodes as shown in Figures 11(a) (cranial-caudal plane) and 11(b) (medial-lateral plane).

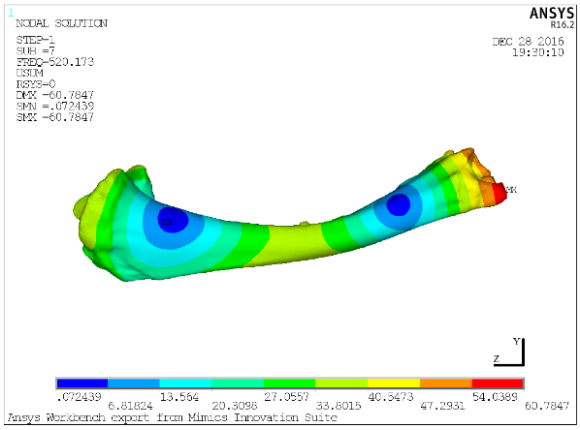

1st Mode

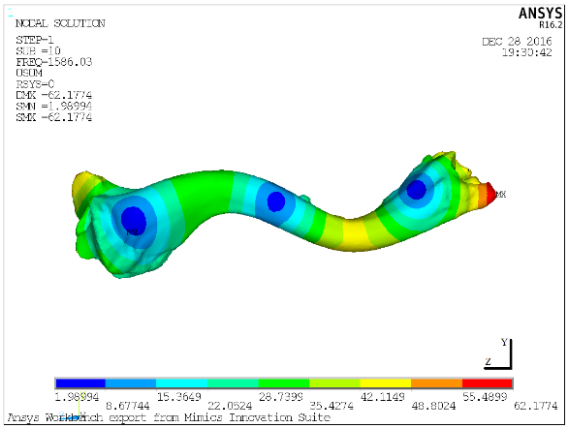

2nd Mode

(a)

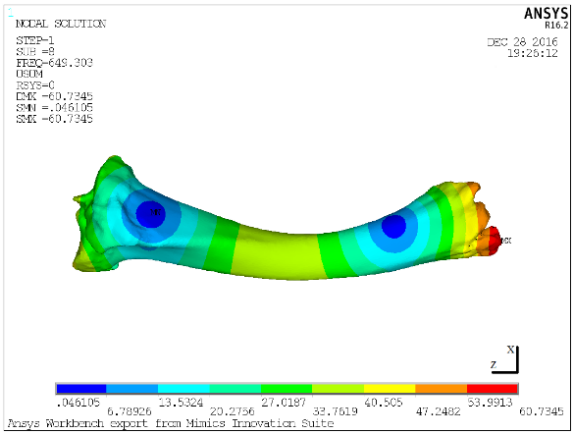

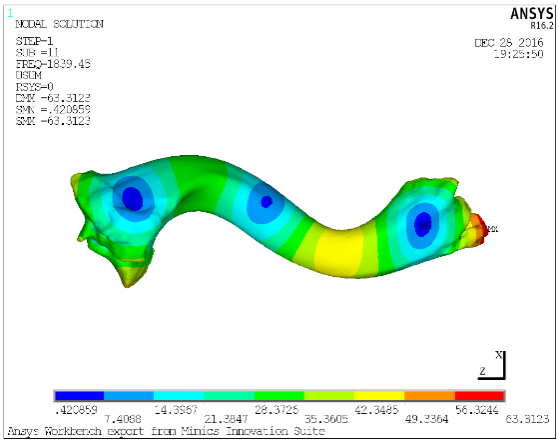

1st Mode 2nd Mode

(b)

Figure 11. Mode shapes 1 and 2 for case 12 (Bone A): (a) cranial-caudal and (b) medial-lateral plane.

3. *Histogram plots: Stiffness vs number of elements*

To illustrate the consequence of modulus-density formula applicable ranges based on the cut-off HU values, we examine the resulting number of elements and their assigned stiffness. Figure 12 shows histograms of stiffness vs. number of elements for cases obtained most-accurate and least-accurate frequency value estimates. Figure 12(a) shows cases 6, 11 and 14 to have cortical bone constituent of lowest stiffness (~11200-15200 MPa) and computed lowest set of modal frequencies. Specifically, case 11 produced very large number of elements of low stiffness (65000 elements having *E*=1600 MPa) and yielded the least mode values ($F_{n_1} = 453.14$ Hz). Over-estimated mode frequencies were obtained for cases 5, 8 and 13 and for which Figure 12(b) shows elemental-modulus to have shifted to the largest stiffness values (~19200 - 23000 MPa). Most accurate estimates resulted from cases of balanced mix of stiffness ranges. Figure 6(c) shows that cases 9, 12 and 15 fit this criterion with cortical modulus in the range of ~14500-20000 MPa. Figure 12(d) illustrates the likely reason being gross imbalance of properties in contrasting case 19 that computed low frequencies ($F_{n_1} = 453.88$ Hz) with case 12 being one of the best cases. Figure 12(e) presents the cases with power cortical equation referenced to the same literature as that of cases 9, 12 and 15 but with a linear relation. However, cases 9, 12 and 15 have higher number of elements for cortical stiffness for approximate 19000 MPa. This results with lower modal frequencies.

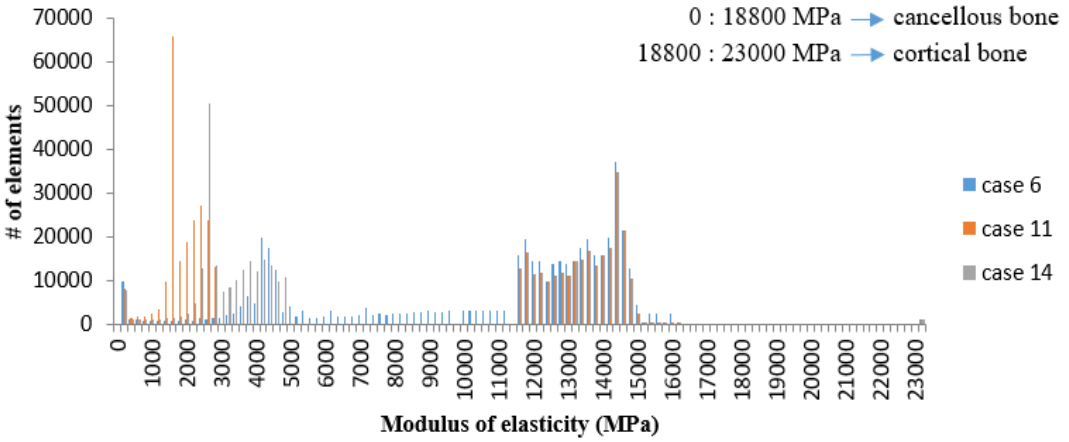
0 : 18800 MPa → cancellous bone
18800 : 23000 MPa → cortical bone
case 6
case 11
case 14
# of elements
Modulus of elasticity (MPa)

(a)

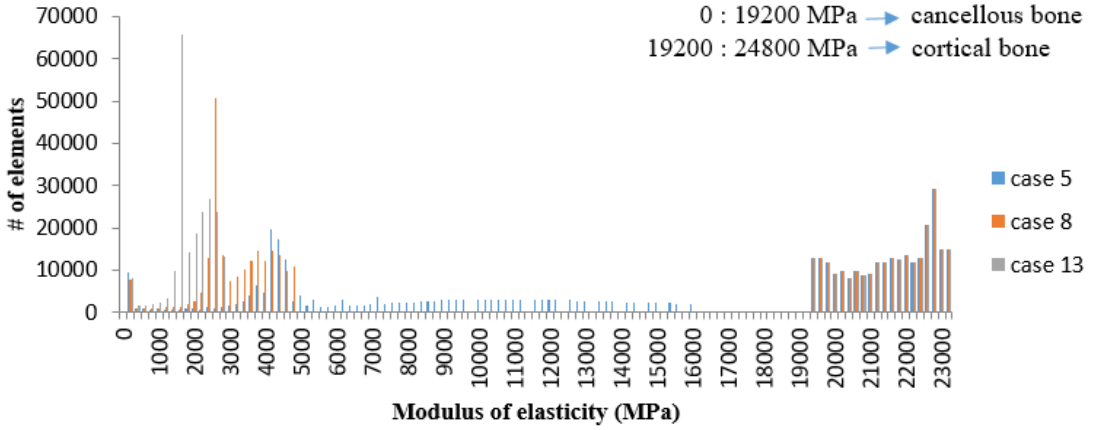
0 : 19200 MPa → cancellous bone
19200 : 24800 MPa → cortical bone
case 5
case 8
case 13
# of elements
Modulus of elasticity (MPa)

(b)

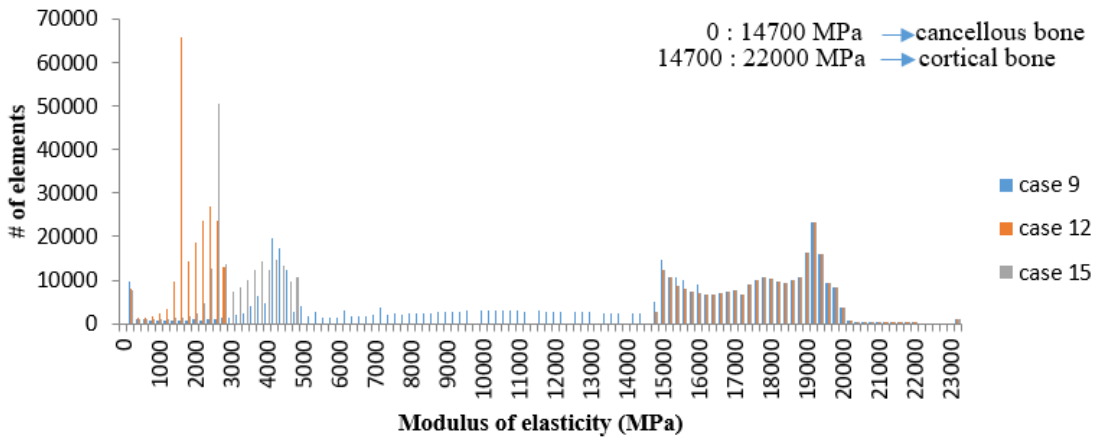
0 : 14700 MPa → cancellous bone
14700 : 22000 MPa → cortical bone
case 9
case 12
case 15
# of elements
Modulus of elasticity (MPa)

(c)

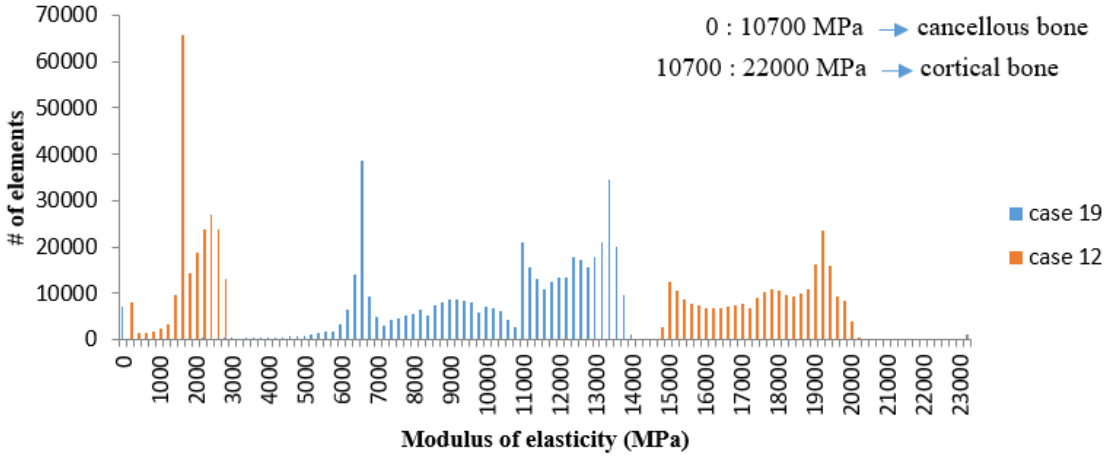

(d)

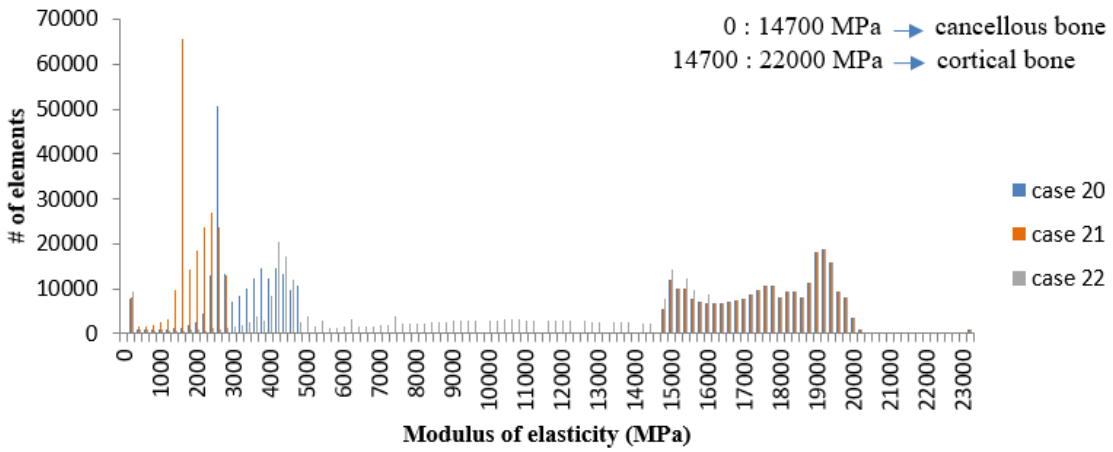

(e)

Figure 12. Histograms showing modulus properties with respect to their relative assigned number of elements: (a) cases 6, 11 and 14, (b) cases 5, 8 and 13, (c) cases 9, 12 and 15, (d) cases 12 and 19, and (d) cases 20, 21 and 22.

C. Numerical vs. Experimental Results (Modal Frequencies and Shapes)

The percentage differences between numerical and experimental data are listed in Table 8. For cases that computed most satisfactory outcomes, comparing results yielded a norm percentage difference of 0.95 % for mode 1 and 10.65 % for mode 2,

and 8.89 % for mode 1 and 1.92 % for mode 2, in the cranial-caudal and medial-lateral planes, respectively.

Table 8. Values and percentage difference between numerical and experimental outcomes for the best three cases found (bone A).

Case #	Cranial-Caudal Plane		Medial-Lateral Plane	
	1st Mode (Hz)	2nd Mode (Hz)	1st Mode (Hz)	2nd Mode (Hz)
Case 9	531.77	1664	666.01	1938.5
Case 12	520.17	1586	649.3	1839.4
Case 15	524.4	1613.5	655.32	1873.4
Experimental	521	1465	721	1865
Total average percentage difference (%)	0.95	10.65	8.89	1.92

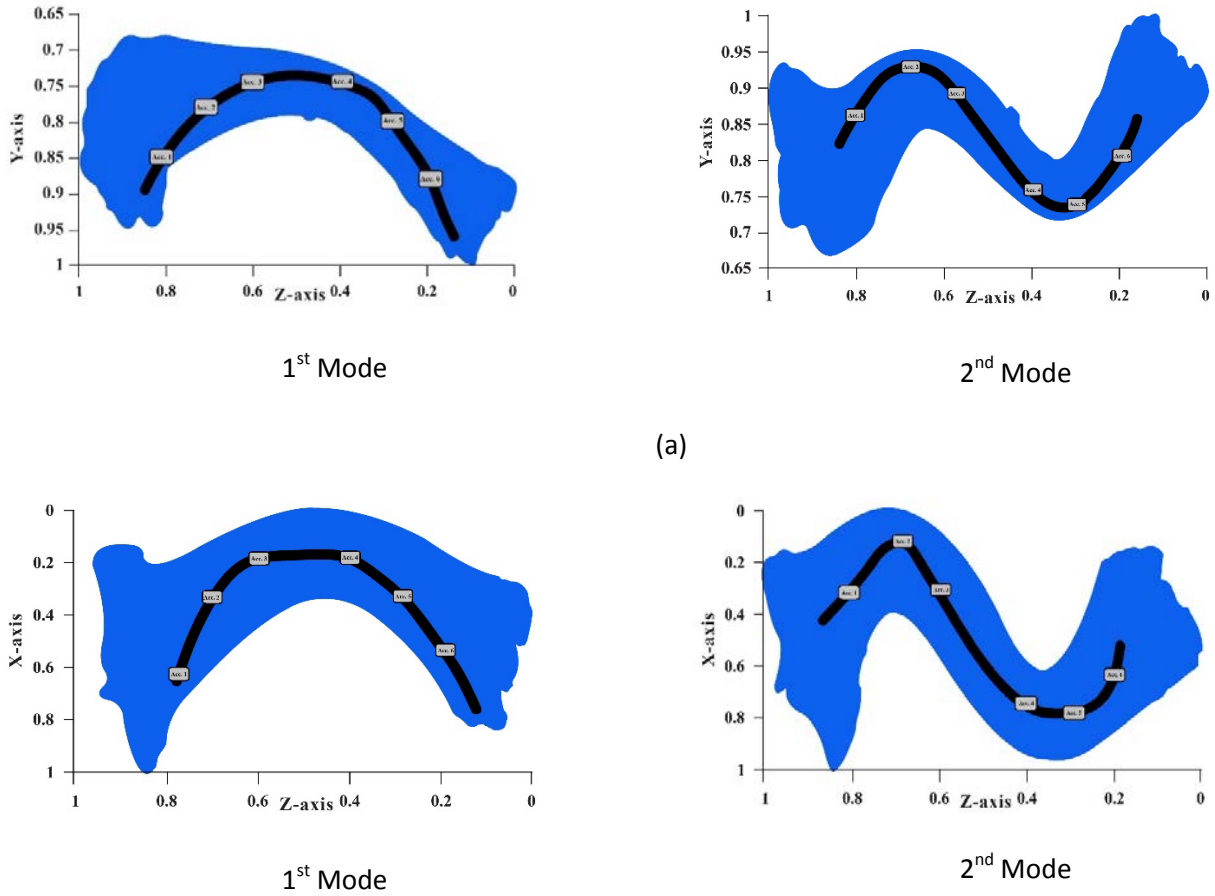

Figure 13. Numerical and experimental shapes mode 1 (left) and mode 2 (right) of tibia Bone A in (a) cranial-caudal and (b) medial-lateral planes (in mm). (x and z-axis refer to Figure 1)

Mode shapes are experimentally revealed as measured by FRF. ProSig© revealed the modal frequencies where the circle fit method is used for extracting modal shapes. Experimental and numerical (FEM) mode shapes revealed similar profiles and are shown superimposed in Figure 13 (a) and (b) for modes 1 and 2.

D. Test Case Verification: Uncharacterized Bone B

For further corroboration, the same technique used for the analysis of the long bone above (Bone A) was repeated in this section on a different long bone, Bone B. The

FEM model is composed of 317107 linear tetrahedral (Tet 4) elements and 54124 nodes. Given the efficacy of the methodology outlined above, the measured and FEM-estimated mass for Bone B are 916 and 913.56 kg, respectively (only 0.26 % difference). Numerical results for Bone B are listed in Table 9 for the three best cases: 9, 12, and 15. (Although FEM-produced modal shapes and frequency values like Figure 3 are available, they are not shown for space limitations). Good agreement is found between numerical results and experimental measurements (also not shown) with (average) difference values of 4.75 % and 1.83 % for modes 1 and 1.88 % and 2.48 % for modes 2, for cranial-caudal and medial-lateral planes, respectively.

Table 9. Frequency value results for Bone B

Case #	Weighted average modulus of Elasticity (MPa)	Cranial-Caudal Plane		Medial-Lateral Plane	
		1st Mode (Hz)	2nd Mode (Hz)	1st Mode (Hz)	2nd Mode (Hz)
Case 9	10460.65	615.33	1833.6	820.59	2298.5
Case 12	8879.52	608.04	1762.8	806.65	2194.6
Case 15	9376.74	611.79	1798.9	813.71	2245.9
Experimental		584	1770	828.80	2192.0
Total average percentage difference (%)		4.75	1.88	1.83	2.48

E. Modeling of Modal Frequency Values

In this section, models are developed in order to produce equations capable of estimating modal frequency values of the long bones (within the range of experimental considerations in this study). A statistical diagnosis is run employing IBM SPSS Statistics to identify the most salient variables affecting the bone dynamic characteristics. Table 10 is the correlation matrix listing collinearity values amongst all

10 variables identified in Table 1. Some parameter combinations were found to be highly correlated including: mass / CC proximal, mass / d_{CC}, mass / area, CCproximal / MLdistal, and CCdistal / d_{ML}. For example, given that area and perimeter are function of d_{ML} and d_{CC}, Pearson coefficient of 0.9896 is found to correlate area with perimeter, and a 0.8754 and 0.945 was found between perimeter, d_{CC} and d_{ML}, respectively. Variables found to be statistically redundant were subsequently eliminated.

Table 10. Correlation matrix using the Pearson correlation coefficient.

Variable	Length	Mass	CC proximal	ML proximal	CC distal	ML distal	d_{CC}	d_{ML}	Area
Mass	0.8345								
CC proximal	0.7271	0.8232							
ML proximal	0.5571	0.4647	0.7537						
CC distal	0.2071	0.5324	0.7042	0.2375					
ML distal	0.5932	0.5852	0.8508	0.6546	0.56				
d_{CC}	0.6002	0.8055	0.7697	0.4187	0.7441	0.5539			
d_{ML}	0.4226	0.7573	0.6868	0.2709	0.8021	0.3196	0.7694		
Area	0.5631	0.8402	0.757	0.3649	0.7924	0.4107	0.8754	0.945	
Perimeter	0.526	0.8129	0.7423	0.3758	0.7913	0.3959	0.8806	0.9606	0.9896

Only variable combinations having the least Pearson correlations (Length, $ML_{proximal}$, CC_{distal}, ML_{distal}, and perimeter (or d_{ML} or area)) were retained to model the 1st and 2nd bending frequencies in both planes (Table 11).

Table 11. Variables considered and p-values representing statistical significance.

Variable	Mode 1 in CC	Mode 2 in CC	Mode 1 in ML	Mode 2 in ML
Length	0.002	0.357	0.001	0.007
$ML_{proximal}$	0.937	0.973	0.637	0.293
CC_{distal}	0.148	0.649	0.368	0.209
ML_{distal}	0.739	0.692	0.283	0.170
perimeter	0.005	0.672	0.008	0.106

Given the non-statistically significant p-values, Table 11 shows the $ML_{proximal}$, CC_{distal} and ML_{distal} variables to contribute the least to discerning modal frequency values. The "Perimeter" variable showed correspondence to 1st modes only in both normal planes. To the contrary, Length was found to have high correspondence to frequencies (p-value < 0.05) for all modes (except for the 2nd mode in the C-C plane). It was deduced that the length parameter is the most influential parameter on frequency in both planes with all other being eliminated from further consideration.

An increase in the structure's length and mass or a decrease in the structure's material stiffness and cross-sectional dimensions result in a drop in frequency values. Analytical solution [67] for uniform beam held free-free is

$$F_n = C_n\sqrt{\frac{EI}{mL^4}} \quad \text{(Hz)} \tag{10}$$

where

F_n : Modal frequency

C_n : Constant identifying mode number

E: Young's modulus of elasticity

I: Area moment of inertia

M: Mass per unit length

L: Bone length

Based on Equation (11), a linear regression analysis was performed to fit the CMIF-obtained frequency values as function of $\sqrt{\frac{1}{L^4}}$ ($\frac{1}{L^2}$). The results are illustrated in Figure 14 and listed in Table 12. The modelling fits for modes 1 and 2 in both Cranial-Caudal and Medial-Lateral planes were statistically significant as indicated by high

Pearson correlation factor (R) values and low p-value signifying that the found equations mimic the experimental frequency data. The first and second modes in the Cranial-Caudal plane were best fitted as $F_{n_1} = 36966417\frac{1}{L^2} + 361.2456$ (p=0.045) and $F_{n_2} = 1.46 * 10^8\frac{1}{L^2} + 679.673$ (p=0.05) in relation to $\frac{1}{L^2}$, respectively. The first and second modes in the Medial-Lateral plane were best fitted as $F_{n_1} = 68676471\frac{1}{L^2} + 350.8876$ (p=0.01) and $F_{n_2} = 10^8\frac{1}{L^2} + 1318.36$ (p=0.001) in relation to $\frac{1}{L^2}$, respectively. The results in Table 12 are an enhanced version of fits previously reported to similar bones by Hamade and co-workers [22].

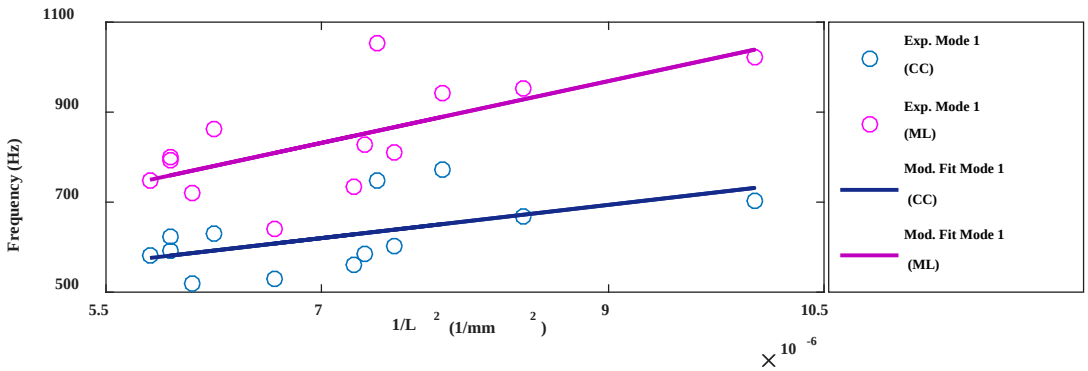

(a)

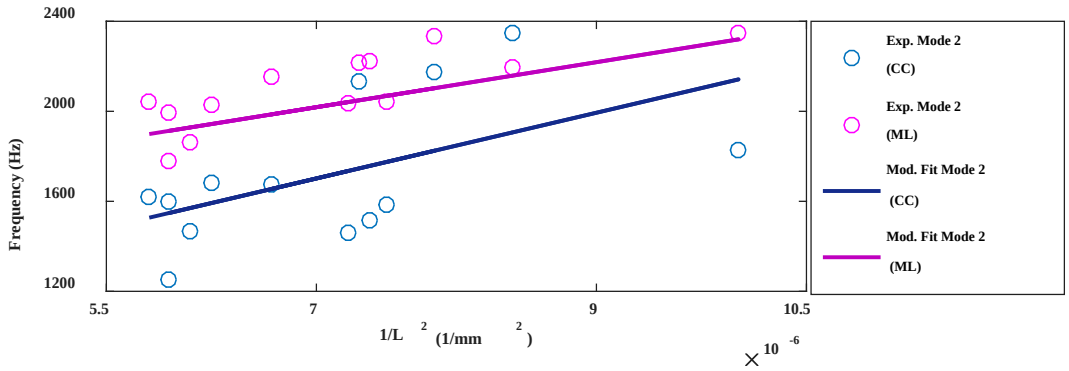

(b)

Figure 14. Fit representations of (a) mode 1 in the Cranial-Caudal and Medial-Lateral planes, (b) mode 2 in the Cranial-Caudal plane and Medial-Lateral plane.

Table 12. Model equations and statistical significance values for Modes 1 and 2 in the Cranial-Caudal and Medial-Lateral planes.

Mode #/Plane	R	p-value	Equation
mode 1(CC)	0.562	0.045	$F_{n_{1CC}} = 36966417\frac{1}{L^2} + 361.2456$
mode 2(CC)	0.548	0.05	$F_{n_{2CC}} = 1.46 * 10^8\frac{1}{L^2} + 679.673$
mode 1(ML)	0.673	0.01	$F_{n_{1ML}} = 68676471\frac{1}{L^2} + 350.8876$
mode 2(ML)	0.778	0.001	$F_{n_{2ML}} = 10^8\frac{1}{L^2} + 1318.36$

CHAPTER VI

CONCLUSION

The modal frequencies in the Cranial-Caudal and Medial-Lateral planes of a large set of 13 long bovine tibias were characterized using Frequency Response Function (FRF) and Complex Mode Indicator Function (CMIF). The bones utilized were acquired from different calves approximately 2 years of age. The impact hammer is a good excitation source to determine the resonant frequencies for small structures, but in case of bones there are some limitations. FRF can result in undependable estimations even if the structure is isolated from external vibrations. The absence of interference in the structure's vibration is typically an arduous duty. For a free-free excited system, the first mode maximally deformed in one location (mid) and the second mode had two maximum deformed positions.

The typical method of analysis uses FRF that may result in varying estimates even if the structure is isolated from external vibrations. CMIF was employed as an alternative method that effectively deals with data subject to noise and distortion. Modes captured using CMIF were fairly close to those measured by FRF. Modes 1 and 2 computed 0.56 % and 2.98 % percentage difference between the two methods in both planes. Upon changing the impact locations, CMIF recorded lower variations in the frequencies than the FRF. The percentage difference was a max of 1.755 % for mode 1 and 5.7 % for mode 2. FRF recorded higher percentages of 1.975 % for mode 1 and 10.905 % for mode 2, in the C-C and M-L planes.

A comprehensive survey of the mechanics' literature revealed twenty two (22) different relationships that estimate the stiffness of cortical and cancellous bone as

function of density. We assess in this work the ability of these formulae to yield accurate FEM predictions of the modal frequencies of long bovine tibia bone in the cranial-caudal and medial-lateral directions. A long tibia bovine bone (Bone A) is dynamically characterized in a free-free boundary experimental setup and the frequency values for which were used as a reference case. Segmentation of CT scans into cortical and cancellous constituents required developing a method for setting a suitable cut-off HU value to demarcate said regions. The study revealed that the 22 assessed formulae yielded greatly varying modal frequencies values with only three $E-\rho$ formulae yielding relatively accurate frequency estimates. On average, these 3 formulae returned frequency values with difference of 0.95 % for 1st mode and 10.65 % for the 2nd mode in the cranial-caudal plane. For verification, procedure was repeated on another test bone (dubbed Bone B) and returned differences of 4.75 % and 1.88 % for the 1st and 2nd cranial-caudal modes, respectively. Stiffness-density formulae that returned the most accurate frequency estimates appear to have produced a balanced distribution of finite elements with stiffness properties congruent with their cancellous or cortical demarcations.

In modelling modal frequencies, the diagnostic study found that the length parameter is the most statistically significant effect by which a change in the bone length mostly influences a change in modal frequencies (p-value < 0.05 for 3 modes). This was deduced, after testing for collinearity and correspondence among all geometrical dimensions. The geometrical model was found to be statistically significant for modal estimation in relating modal frequencies to the reciprocal of the length squared for different modes and planes. For all 4 cases, the p-value was found to be significant ($0.001 < p \leq 0.05$) with high correlation factors (~ 55 < R < 78%).

REFERENCES

[1] Daggett, W. M. and W. G. Austen (1967). Symposium on Biomedical Engineering and SurgeryBiomedical engineering applications to cardiovascular surgery. *The American Journal of Surgery*, 114(1), 139-149.

[2] Van der Perre, G. and G. Lowet (2006). In vivo assessment of bone mechanical properties by vibration and ultrasonic wave propagation analysis. *Bone*, 18(1), S29-S35.

[3] Doherty, W.P. (1971). Dynamic response of human tibiae-application to fracture healing and osteoporosis. Ph.D. Thesis, U.C. Berkeley.

[4] Doherty, W.P., Bovil, E., Wilson, E. (1974). Evaluation of the use of resonant frequencies to characterize physical properties of human long bones. *Journal of Biomechanics*, 7, 559-561.

[5] Sonstegard, D. A. and Matthews, L. S. (1976). Sonic diagnosis of bone fracture healing-- A preliminary study. *Journal of Biomechanics*, 9, 689-4594.

[6] Duchemin, L., Bousson, V., Roassanaly, C., Bergot, C., Laredo, J. D., Skalli, W., Mitton, D. (2008). Prediction of mechanical properties of cortical bone by quantitative computed tomography. *Medical Engineering & Physics*, 30(3), 321-328.

[7] Taylor, W. R., Roland, E., Ploeg, H., Hertig, D., Klabunde, R., Warner, M. D., Hobatho, M. C., Rakotomanana, L., Clift, S.E. (2002). Determination of orthotropic bone elastic constants using FEA and modal analysis. *Journal of Biomechanics*, 35(6), 767-773.

[8] Lee, J. W., Kim, K. J., Kang, K. S., Chen, S., Rhie, J. W., Cho, D. W. (2013). Development of a bone reconstruction technique using a solid free-form fabrication (SFF)-based drug releasing scaffold and adipose-derived stem cells. *Journal of Biomedical Materials Research Part A*, 101(7), 1865–1875.

[9] Scholz, R., Hoffmann, F., Von Sachsen, S., Drossel, W.G., Klohn, C., Voigt, C., (2013). Validation of density-elasticity relationships for finite element modeling of human pelvic bone by modal analysis. *Journal of Biomechanics*, 46(15), 2667-2673.

[10] Di Puccio, F., Mattei, L., Longo, A., Marchetti, S. (2017). Fracture Healing Assessment Based on Impact Testing: In Vitro Simulation and Monitoring of the Healing Process of a Tibial Fracture with External Fixator. *International Journal of Applied Mechanics*, 9(7), 1750098.

[11] Hobatho, M. C., Darmana, R., Pastor, P., Barrau, J. J., Laroze, S., and Morucci, J. P. (1991). Development of a Three Dimensional Finite Element Model of a Human Tibia Using Experimental Modal Analysis. *Journal of Biomechanics*, 24(6), 371–383.

[12] Thomsen, J. J. (1990). Modelling human tibia structural vibrations. *Journal of Biomechanics*, 23(3), 215-228.

[13] Gupta, A., and Tse, K. M. (2013). Finite Element Analysis on Vibration Modes of Femur Bone. *International Conference on Advances in Mechanical Engineering (AME)*, NCR, India, Dec. 10–13, 827–831.

[14] Kumar, A., Jaiswal, H., Garg, T., Patil, P. P. (2014). Free vibration modes analysis of femur bone fracture using varying boundary conditions based on FEA. *3rd International Conference on Materials Processing and Characterization (ICMPC 2014). Procedia Materials Science*, 6, 1593-1599.

[15] Liao, Z., Chen, J., Zhang, Z., Li, W., Swain, M., Li, Q. (2015). Computational modeling of dynamic behaviors of human teeth. *Journal of Biomechanics*, 48(16), 4214-4220.

[16] Al Sukhun, J., Kelleway, J., Helenius, M. (2007). Development of a three-dimensional finite element model of a human mandible containing endosseous dental implants. I. Mathematical validation and experimental verification. *Journal of Biomedical Materials Research Part A*, 80(1), 234-246.

[17] Yassine, R. A., Elham, M. K., Mustapha, S., Hamade. R. F. (2018). Heterogeneous Versus Homogeneous Material Considerations in Determining the Modal Frequencies of Long Tibia Bones. *Journal of Engineering in Medical Diagnostics and Therapy*, 1(021001), 1-5.

[18] Phillips, A.W., Allemang, R.J. (1998). The Complex Mode Indicator Function (CMIF) as a Parameter Estimation Method. *Proceedings, International Modal Analysis Conference*, 705-710.

[19] Shih, C.Y., Tsuei, Y.G., Allemang, R.J., and Brown, D.L. (1988). A Frequency Domain Global Parameter Estimation Method for Multiple Reference Frequency Response Measurements. *Mechanical Systems and Signal Processing*, 2(4), 367-377.

[20] Malekian, M., Trieu, D., Owoc, J. S., Park, S. S. (2010). Investigation of the Intervertebral Disc and Fused Joint Dynamics through Experimental Modal Analysis and the Receptance Coupling Method. *Journal of Biomechanical Engineering*, 132, 041004-1-13.

[21] Mimics student edition course book, Innovation Suite Research, Materialize Technologielaan 15 – 3001 Leuven-Belgium, http://www.materialise.com/en/medical/software/mimics, Accessed January 10, 2017.

[22] Choucair, I., Mustapha, S., Fakhreddine, A., Sayegh, M., and Hamade, R. F. (2016). Investigation of the Dynamic Characteristics of Bovine Tibia Using the Impulse Response Method. *ASME Paper* No. IMECE2016-66554.

[23] Yassine, R., Fakhreddine, A., Sayegh, M., Mustafa, S., Hamade, R. (2018). Dynamic Assessment and Modelling of the Modal Frequencies and Shapes of Bovine Tibia. *Journal of Nondestructive Evaluation, Diagnostics and Prognostics of Engineering* (not published).

[24] Van der Perre, G., Van Audekercke, R., Martens, M., Mulier, J. C. (1983). Identification of In-Vivo Vibration Modes of Human Tibiae by Modal Analysis. *Journal of Biomechanical Engineering*, 105, 244-248.

[25] Cornelissen, P., Cornelissen, M., Van Der Perre, G., Christensen, A.B., Ammitzvoll, F., Dyrbye, C. (1986). Assessment of tibial stiffness by vibration testing in situ—II. Influence of soft tissues, joints and fibula. *Journal of Biomechanics*, 19 (7), 551-561.

[26] Lowet, G., Van Audekercke, R., Van der Perre, G., Geusens, P., Dequeker, J., Lammens, J. (1993). The Relation between Resonant Frequencies and Torsional Stiffness of Long Bones In Vitro. Validation of a Simple Beam Model. *Journal of Biomechanics*, 26(6), 689-696.

[27] Christensen, A. B., Ammitzboll, F., Dyrbye, C., Cornelissen, M., Cornelissen, P., Van der Perrre, G. (1986). Assessment of Tibial Stiffness by Vibration Testing In Situ – I. Identification of Mode Shapes in Different Supporting Conditions. *Journal of Biomechanics*, 19(1), 53-60.

[28] Nakatsuchi, Y., Tsuchikane, A., Nomura, A. (1996). The Vibrational Mode of the Tibia and Assessment of Bone Union in Experimental Fracture Healing using the Impulse Response Method. *Medical Engineering & Physics*, 18(7), 575-583.

[29] Alizad, A., Walch, M., Greenleaf, J. F., Fatemi, M. (2006). Vibrational Characteristics of Bone Fracture and Fracture Repair: Application to Excised Rat Femur. *Journal of Biomechanical Engineering*, 128, 300-308.

[30] Nokes, L., Mintowt-Czyz, W. J., Fairclough, J. A., Mackie, I., Williams, J. (1985). Vibration Analysis in the Assessment of Conservatively Managed Tibial Fractures. *Journal of Biomedical Engineering*, 7(1), 40-44.

[31] Hight, T. K., Piziali, R. L., Nagel, D. A. (1980). Natural Frequency Analysis of a Human Tibia. *Journal of Biomechanics*, 13(2), 139-147.

[32] Collier, R. J., Nadav, O., Thomas, T. G. (1982). The Mechanical Resonances of a Human Tibia: Part I - In Vitro. *Journal of Biomechanics*, 15(8), 545-553.

[33] Wang, H. and K. Williams (1996). Vibrational modes of thick cylinders of finite length. *Journal of Sound and Vibration*, 191(5), 955-971.

[34] Makki Alamdari, M., Li, J., Samali, B. (2014). FRF-Based Damage Localization Method with Noise Suppression Approach. *Journal of Sound and Vibration*, 333(14), 3305-3320.

[35] Banks, H. T., Inman, D. J., Leo., D. J., Wang, Y. (1996). An Experimentally Validated Damage Detection Theory in Smart Structures. *Journal of Sound and Vibration*, 191(5), 859-880.

[36] Liu, J., Zhang, Y., Yun, B. (2012). A New Method for Predicting Nonlinear Structural Vibrations Induced by Ground Impact Loading. *Journal of Sound and Vibration*, 331, 2129-2140.

[37] Rade, M. (2010). Performance of Various Mode Indicator Functions. *Shock and Vibration*, 17(4-5), 473-482.

[38] Phillips, A.W., Allemang, R. J. (2004). The Unified Matrix Polynomial Approach to Understanding Modal Parameter Estimation: An Update. Proceedings, International Conference on Noise and Vibration Engineering, Katholieke Universiteit Leuven, Belgium 36.

[39] Shih, C. Y., Tsuei, Y. G., Allemang, R. J., Brown, D. L. (1988). Complex Mode Indication Function and Its Applications to Spatial Domain Parameter Estimation. *Mechanical Systems and Signal Processing*, 2(4), 367-377.

[40] Snyder, S. M., and Schneider, E. (1989). Estimation of Mechanical Properties of Cortical Bone by Computed Tomography. *Journal of Orthopaedic Research*, 9(3), 422–431.

[41] Lotz, J. C., Gerhart, T. N., Hayes, W. C. (1991). Mechanical properties of metaphyseal bone in the proximal femur. *Journal of Biomechanics*, 24(5), 317-329.

[42] Keaveny, T. M., Morgan, E. F., Niebeur, G. L., Yeh, O.C. (2001). Biomechanics of trabecular bone. *Annual Review of Biomedical Engineering*, 3, 307-333.

[43] Gupta, S., and Dan, P. (2004). Bone Geometry and Mechanical Properties of the Human Scapula Using Computed Tomography Data. *Biomaterials for Artificial Organs*, 17(2), 61–70.

[44] Wirtz, D. C., Schiffers, N., Pandorf, T., Radermacher, K., Weichert, D., Forst, R. (2000). Critical evaluation of known bone material properties to realize anisotropic FE-simulation of the proximal femur. *Journal of Biomechanics*, 33(10), 1325-1330.

[45] Abendschein, W., Hyatt, G.W. (1970). Ultrasonics and selected physical properties of bone. *Clinical Orthopaedics and Related Research*, 69, 294-301.

[46] Austman, R. L., Milner, J. S., Holdsworth, D. W., Dunning, C. E. (2009). Development of a customized density-modulus relationship for use in subject-specific finite element models of the ulna. *Proceedings of the institution of Mechanical Engineers*, 223(6), 787-794.

[47] Austman, R. L., Milner, J. S., Holdsworth, D. W., Dunning, C. E. (2008). The effect of the density-modulus relationship selected to apply material properties in a finite element model of long bone. *Journal of Biomechanics*, 41(15), 3171-3176.

[48] Morgan, E. F., Bayraktar, H. H., Keaveny, T. M. (2003). Trabecular bone modulus-density relationships depend on anatomic site. *Journal of Biomechanics*, 36(7), 897-904.

[49] Carter, D. R., and Hayes, W. C. (1977). The Compressive Behavior of Bone as a Two-Phase Porous Structure. *The Journal of Bone and Joint Surgery Ser. A*, 59(7), 954–962.

[50] Schileo, E., Taddei, F., Malandrino, A., Cristofolini, L., Viceconti, M. (2007). Subject-specific finite element models can accurately predict stain levels in long bones. *Journal of Biomechanics*, 40(13), 2982-2989.

[51] Huang, H. L., Tsai, M. T., Lin, D. J., Chien, C. S., Hsu, J. T. (2010). A new method to evaluate the elastic modulus of cortical bone by using combined computed

tomography and finite element approach. *Computers in Biology and Medicine*, 40(4), 464-468.

[52] Malekian, M., Trieu, D., Owoc, J. S., Park, S. S. (2010). Investigation of the Intervertebral Disc and Fused Joint Dynamics through Experimental Modal Analysis and the Receptance Coupling Method. *Journal of Biomechanical Engineering*, 132 041004-1-13.

[53] Carne, T. G., Griffith, D. T., Casias, M. E. (2007). Support Conditions for Experimental Modal Analysi. *Sound and Vibration*, 41(6), 10-16.

[54] Utz, J. C., Nelson, S., O'Toole, B. J., Van Breukelen, F. (2009). Bone Strength is Maintained after 8 Months of Inactivity in Hibernating Golden-Mantled Fround Squirrels, Spermophilus Lateralis. *Journal of Experimental Biology*, 212(17), 2746-2752.

[55] Wren, J. (2009). A Simple Frequency Response Function. http://blog.prosig.com/2009/10/19/a-simple-frequency-response-function/.

[56] Allemang, R. J., Brown, D. L. (2006). A Complete Review of the Complex Mode Indicator Function (CMIF) with Applications. Proceedings, international conference on noise and vibration engineering (ISMA), Katholieke Universiteit Leuven, Belgium 38.

[57] Yassine, R., Elham, M. K., Mustafa, S., and Hamade, R. (2017). A Detailed Methodology for FEM Analysis of Long Bones From CT Using Mimics. *ASME Paper* No. IMECE2017-72571.

[58] Reilly, D. T. and Burstein, A. (1975). The elastic and ultimate properties of compact bone tissue. *Journal of Biomechanics*, 8(6), 393-405.

[59] Zysset, P. K., Guo, X. E., Hoffler, C. E., Moore, K. E., Goldstein, S. A. (1992). Elastic modulus and hardness of cortical and trabecular bone lamellae measured by nanoindentation in the human femur. *Journal of Biomechanics*, 32(10), 1005-1012.

[60] Sitzer, A., Wendlandt, R., Barkhausen, J., Kovacs, A., Weyers, I., Schulz, A. P. (2012). Determination of Material Properties Related to Quantitative CT in Human Femoral Bone for Patient Specific Finite Element Analysis - A Comparison of Material Laws. *ORTHOPAEDICS*, 3(7), WMC003456.

[61] Kohles, S. S. (2000). Application of an anisotropic parameter to cortical bone. *Journal of Materials Science: Materials in Medicine*, 11(4), 226-265.

[62] Novitskaya, E., Chen, P., Lee, S., Castro-Cesena, A., Hirata, G., Lubardo, V., McKittrick, J. (2011). Anisotropy in the compressive mechanical properties of bovine cortical bone and the mineral and protein constituents. *Acta Biomaterialia*, 7(8), 3170-3177.

[63] Hage, I. S., Seif, C. Y., and Hamade, R. F. (2016). Measuring Compressive Modulus of Elasticity Across Cortical Bone Thickness of Mid-Diaphysis Bovine Femur. *ASME Paper* No. IMECE2016-66383.

[64] Knets, I. V., Pfafrod, G. O., Saulgozis, J. Z. (1980). Deformation and fracture of hard biological tissue. Zinatne, Riga, 319.

[65] Fatehi, P. and Nejad, M. Z. (2014). Effects of material gradients on onset of yield in FGM rotating thick cylindrical shells. *International Journal of Applied Mechanics*, 6(4), 1450038.

[66] Lee, J. W., Kim, K. J., Kang, K. S., Chen, S., Rhie, J. W., Cho, D. W. (2013). Development of a bone reconstruction technique using a solid free-form fabrication (SFF)-based drug releasing scaffold and adipose-derived stem cells. *Journal of Biomedical Materials Research Part A*, 101(7), 1865–1875.

[67] Mahmoud, A. A., Abdelghany, S. M., Ewis, K. M. (2013). Free Vibration of Uniform and Non-Uniform Euler Beams using the Differential Transformation Method. *Asian Journal of Mathematics and Applications*, 1-16.

[68] Linde, F., Hvid, I., Madsen, F. (1992). The effect of specimen geometry on the mechanical behaviour of trabecular bone specimens. *Journal of Biomechanics*, 25(4), 359-368.